JCB Journal of Cell Biology

ARTICLE

CD2AP links actin to PI3 kinase activity to extend epithelial cell height and constrain cell area

Yuou Wang and William M. Brieher

Maintaining the correct ratio of apical, basal, and lateral membrane domains is important for epithelial physiology. Here, we show that CD2AP is a critical determinant of epithelial membrane proportions. Depletion of CD2AP or phosphoinositide 3-kinase (PI3K) inhibition results in loss of F-actin and expansion of apical–basal domains, which comes at the expense of lateral membrane height in MDCK cells. We demonstrate that the SH3 domains of CD2AP bind to PI3K and are necessary for PI3K activity along lateral membranes and constraining cell area. Tethering the SH3 domains of CD2AP or p110γ to the membrane is sufficient to rescue CD2AP-knockdown phenotypes. CD2AP and PI3K are both upstream and downstream of actin polymerization. Since CD2AP binds to both actin filaments and PI3K, CD2AP might bridge actin assembly to PI3K activation to form a positive feedback loop to support lateral membrane extension. Our results provide insight into the squamous to cuboidal to columnar epithelial transitions seen in complex epithelial tissues in vivo.

Introduction

Epithelial cells line all organs, body cavities, lumens, and ducts. They mediate the selective transport of materials from one side of the epithelial barrier to the other. To perform these functions, epithelial cells must build three distinct membranes, apical, lateral, and basal, each of which performs different functions. The composition of each membrane domain is tightly regulated and varies between different types of epithelial cells to meet physiological demands (Caceres et al., 2017). The size of each membrane domain also varies between cell types in accordance with the underlying physiology, and while epithelia can selectively control the size of each membrane domain, it is the height of the lateral membrane that is used to categorize epithelia into squamous versus cuboidal versus columnar morphologies (Lowe and Anderson, 2015).

The height of the lateral membrane is connected to cell function. For example, type 1 alveolar epithelial cells in lung are very thin (squamous) to facilitate gas exchange (Bertalanffy and Leblond, 1955; Guillot et al., 2013). Such cells build a short lateral membrane. Other cell types, like the transporting epithelial cells in the kidney, build taller lateral membranes in order to increase the number of transport proteins in the lateral membrane to increase transcellular flux of specific solute molecules through the epithelial barrier (Larsson et al., 1983; Zhai et al., 2003, 2006). While the height of lateral membrane is closely connected to cell function, little is known about what controls it. This is bound to be a complicated problem involving specific transcription factors, adhesion molecules, polarized membrane trafficking, cytoskeletal organization, and the signaling feedback loops that control them (Tang, 2017).

Earlier work identified phosphoinositide 3-kinase (PI3K) and its product, Pins(3,4,5)P_3, as important determinants of lateral membrane height (Gassama-Diagne et al., 2006; Jeanes et al., 2009), but how PInsP$_3$ production leads to extension of the lateral membrane is not known. Modulation of the actin cytoskeleton is a strong possibility. Certain actin binding proteins, such as ankyrin, spectrin (He et al., 2014; Jenkins et al., 2015; Kizhatil et al., 2007), and tropomodulin (Weber et al., 2007), are important for maintaining the height of lateral membranes. Actin assembly factors, including EVL, CRMP1, Arp2/3, WAVE2, and myosin 1c, are also important for extension of the lateral membrane (Kannan and Tang, 2015, 2018; Yu-Kemp et al., 2017). Finally, rho and p120 catenin, which helps control rho activity (Noren et al., 2000), are both implicated in lateral membrane extension (Yu et al., 2016). Since PI3K plays an important role in building the actin cytoskeleton in different cell types (Cain and Ridley, 2009), it is possible that PI3K's effect on cell height is due, at least in part, to its effects on actin.

The connection between PI3K and actin is best understood in amoeboid cells, where PI3K activation triggers Arp2/3-dependent actin polymerization to generate a protruding leading edge as part of directional cell migration toward a chemotactic signal (Cain and Ridley, 2009; Funamoto et al., 2001, 2002; Hannigan

Department of Cell and Developmental Biology, University of Illinois, Urbana-Champaign, Urbana, IL.

Correspondence to William M. Brieher: wbrieher@illinois.edu.

https://doi.org/10.1083/jcb.201812087

et al., 2002; Weiger and Parent, 2012). Far less is known about whether PI3K plays a role in actin assembly in normal epithelial cells in which cell motility is largely suppressed. Nevertheless, nontransformed epithelial cells in culture maintain fast actin assembly/disassembly turnover dynamics despite the fact that cells are not moving (Tang and Brieher, 2012). Much of the actin assembly occurring at cell–cell junctions and within the actin cortex is Arp2/3 dependent (Tang and Brieher, 2012, 2013; Van Itallie et al., 2015; Yu-Kemp et al., 2017), and loss of these actin networks often leads to decreased cell height and conversion from a cuboidal to squamous morphology (Tang and Brieher, 2012; Yu-Kemp et al., 2017).

Previously, we identified CD2AP as another protein necessary for assembling the actin cytoskeleton at apical cell–cell junctions as well as the apical actin cortex (Tang and Brieher, 2013). CD2AP's positive effect on actin assembly in cells is paradoxical, because CD2AP itself suppresses actin polymerization in vitro, but this could be an epiphenomenon (Tang and Brieher, 2013). How CD2AP promotes actin assembly in cells is complicated, because CD2AP is modular protein that binds to several other partners through CD2AP's three SH3 domains, its proline-rich domain, and other small motifs and regions (Dustin et al., 1998). Some of CD2AP's binding partners include cortactin (Lynch et al., 2003; Zhao et al., 2013), anillin (Monzo et al., 2005), and capping protein (Bruck et al., 2006; Hernandez-Valladares et al., 2010; Hutchings et al., 2003). These interactions might explain how CD2AP promotes actin assembly in cells. Alternatively, CD2AP's potent effect on actin assembly in cells might be due to interactions with PI3K. CD2AP binds to the p85α regulatory subunit of PI3K, and it helps recruit PI3K to the plasma membrane in podocytes (Huber et al., 2003; Ren and You Yu, 2016). Given the importance of CD2AP in junctional actin assembly and epithelial barrier function (Cochran et al., 2015; Tang and Brieher, 2013), inherited kidney disease (Kim et al., 2003; Shih et al., 1999), and possibly Alzheimer's disease (Cochran et al., 2015 Hollingworth et al., 2011; Naj et al., 2011), we reinvestigated the role of CD2AP in junctional actin assembly. That line of investigation led us to discover an important role for CD2AP in phosphatidylinositol (3,4,5)-trisphosphate ($PI(3,4,5)P_3$) synthesis and epithelial cell height.

Results

CD2AP depletion reduced total F-actin accumulation and altered cell morphology

Previous work showed that disrupting actin assembly along lateral membranes and within the apical actin cortex by depleting MDCK cells of CRMP1, EVL, WAVE2, or Arp2/3 results in large changes in cell area with a reduction in cell height (Yu-Kemp et al., 2017). CD2AP is also responsible for F-actin accumulation at cell–cell junctions, along lateral membranes, and in the apical actin cortex (Tang and Brieher, 2013). To test if CD2AP is also involved in epithelial cell morphology regulation, shCD2AP-MDCK cells were generated. The morphology of CD2AP depleted cells was compared with that of control cells using fluorescently tagged phalloidin to stain for F-actin, which also allowed us to compare actin polymer levels as well as view the overall size and shape of the cells. WT-MDCK cells showed brighter F-actin staining at cell–cell borders and within the apical membrane cortex than CD2AP-depleted cells. (Fig. 1 A). Immunofluorescence imaging of CD2AP showed reduced CD2AP content in the shRNA-treated cells (Fig. 1 A, middle). Reduction of CD2AP protein levels by the shRNA was further confirmed by Western blotting, which showed an overall ∼50% reduction in CD2AP relative to control cells (Fig. 1 B). The large drop in actin and CD2AP fluorescence intensity made it difficult to see the outline of the cells and the organization of the actin cytoskeleton that remains following CD2AP knockdown. Therefore, we rescaled the images of the CD2AP-knockdown cells to make them brighter and easier to see the large change in cell area that accompanies loss of F-actin (Fig. 1 A, bottom row). Quantification of F-actin levels from phalloidin-stained cells showed a strong correlation between the level of CD2AP and the level of F-actin both in the apical cell cortex (Fig. 1 C) and at cell–cell boundaries (Fig. 1 D), with the reduced levels of CD2AP in the knockdown cells producing further reductions in F-actin.

Confocal microcopy was then used to assess the morphological changes upon CD2AP knockdown. Cell height and spreading area were measured from xz and xy projections, respectively, of WT-MDCK and shCD2AP cells using F-actin to mark the cell borders. xz projections showed that CD2AP depletion decreased cell height from an average of 3.8 ± 0.6 µm in WT cells to an average of 2.2 ± 0.3 µm in CD2AP-depleted cells corresponding to an ∼40% reduction in cell height (Fig. 1, E and F). The reduction in lateral membrane height was accompanied by an increase in cell spreading area by approximately threefold from an average of 161 ± 69 μm^2 in control cells to 470 ± 112 μm^2 in CD2AP-depleted cells (Fig. 1 G). These data show that CD2AP is required for maintaining F-actin and the proportional relationship between apical–basal surfaces relative to the lateral membrane.

CD2AP regulates cell dimensions independent of cell population control

The change in cell height could be a downstream consequence of there being fewer cells in the monolayer. To test if changes in cell height are due to compressive forces from cell packing density, we compared cell area and cell height in cultures of WT versus shCD2AP cells plated at extremely low seeding density. An ∼5.6-fold increase in cell expansion (xy axis; Fig. 2, A, B, and D) and 1.5-fold decrease in cell height (Fig. 2, C and E) was detected upon CD2AP knockdown in the absence of cell crowding. Thus, CD2AP regulates cell shape independent of cell density.

CD2AP colocalizes with and binds to PI3K p85α at cell–cell boundaries

The flattened cells are reminiscent of PI3K inhibition phenotypes (Gassama-Diagne et al., 2006; Jeanes et al., 2009), suggesting that CD2AP's effect on lateral membrane height might be linked to PI3K activity and $PI(3,4,5)P_3$ synthesis. To further investigate the possible connection between CD2AP and PI3K, we used immunofluorescence to examine the distribution of CD2AP and the p85α subunit of PI3K in confluent sheets of MDCK cells. Both CD2AP and p85α were organized into puncta that

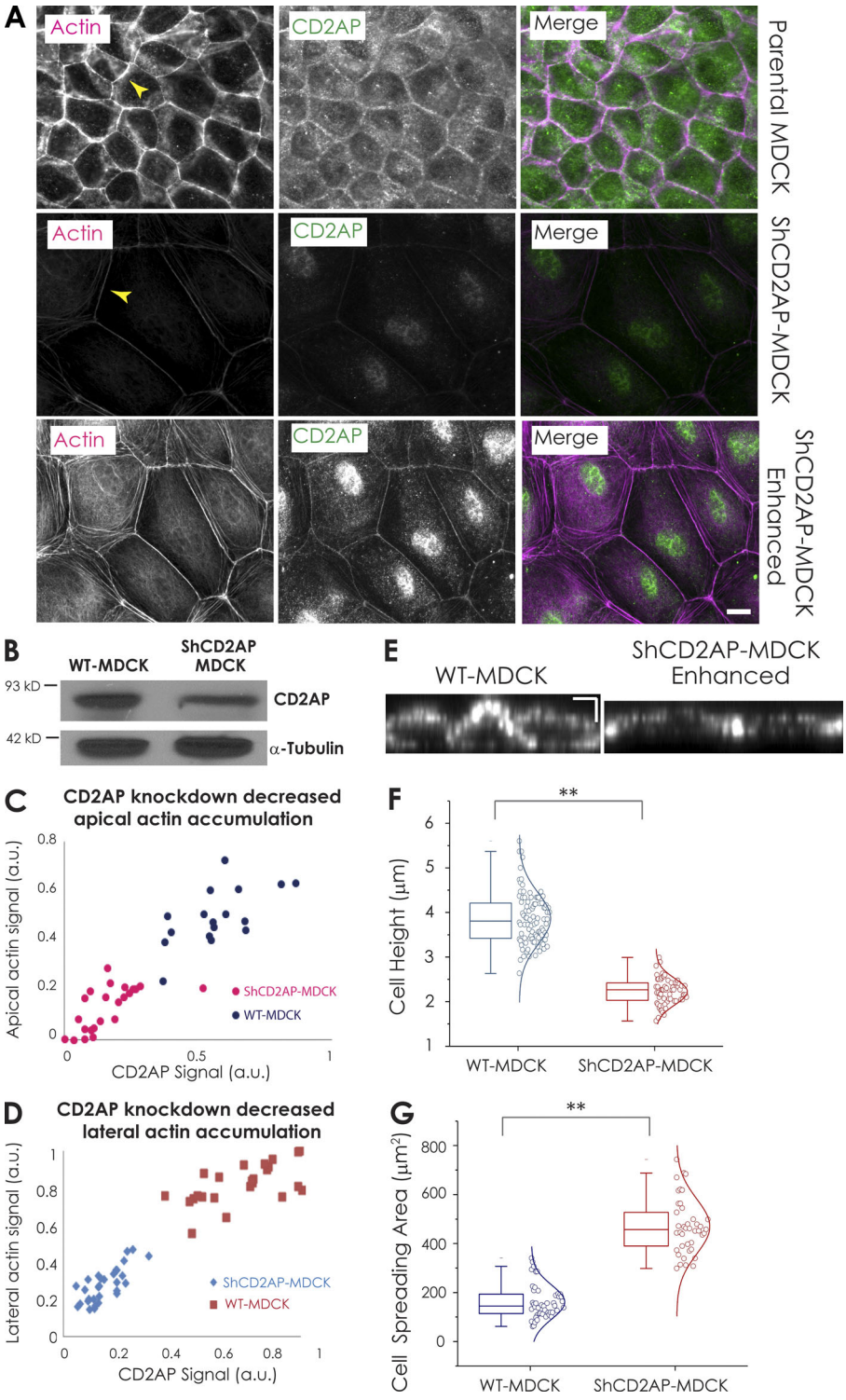

Figure 1. **CD2AP knockdown decreased overall F-actin accumulation and altered cell morphology. (A)** Wide-field immunofluorescence imaging showing CD2AP knockdown diminishes filamentous actin accumulation (arrowheads) and changes cell shape in MDCK cell monolayers. The top panels and middle panels are contrasted the same way to show differences in actin and CD2AP. The contrast in the bottom panels has been enhanced in the CD2AP knockdown cells to better show the residual actin. Scale bar, 10 µm. **(B)** Western blots of total cell extracts showing 50% shRNA knockdown of CD2AP. **(C and D)** Quantification of apical staining (C) and lateral staining (D) of CD2AP and actin (phalloidin) showing a correlation between CD2AP levels and actin levels in both parental and CD2AP knockdown MDCK cells. R^2 = 0.578 lateral-actin to lateral-CD2AP in shCD2AP-MDCK cells; R^2 = 0.3617 lateral-actin to lateral-CD2AP in WT-MDCK cells; R^2 = 0.4025 apical-actin to apical-CD2AP in shCD2AP-MDCK cells; R^2 = 0.3898 apical-actin to apical-CD2AP in WT-MDCK cells. Representative data from three separate experiments are shown. $P < 0.001$ by ANOVA. **(E)** Confocal XZ sections stained with TRITC phalloidin show that CD2AP depletion shortens cell height; the contrast in the right panel has been enhanced. Scale bar, 2.2 µm. **(F and G)** Quantification shows that CD2AP-knockdown results in (F) decreased cell height and (G) increased cell spreading area. **, $P < 0.001$ by ANOVA. Error bars represent SD from three independent experiments.

colocalized along cell–cell contacts in mature MDCK cells (Fig. 3 A). Line scans along the cell–cell boundary confirmed the overlap of CD2AP with PI3K p85α (Fig. 3 B).

Previous results used coimmunoprecipitation and pull-down assays to demonstrate an interaction between CD2AP and PI3K p85α (Huber et al., 2003). We performed microscale thermophoresis (MST) measurements to confirm the association between CD2AP and PI3K p85α and to obtain a dissociation constant. These experiments showed that the N-terminal portion of CD2AP (residues 1–475) bound to PI3K p85α (residues 1–315) with K_d = 0.94 ± 0.41 µM (n = 3; Fig. 3, C and D). Thus, CD2AP physically associates with PI3K p85α and colocalizes with it at cell–cell boundaries in epithelial cells.

PI(3,4,5)P_3 synthesis and PI3K membrane recruitment is diminished in CD2AP knockdown MDCK cells

We used immunofluorescence to test if CD2AP was necessary for recruiting PI3K to membranes and cell–cell boundaries. As shown

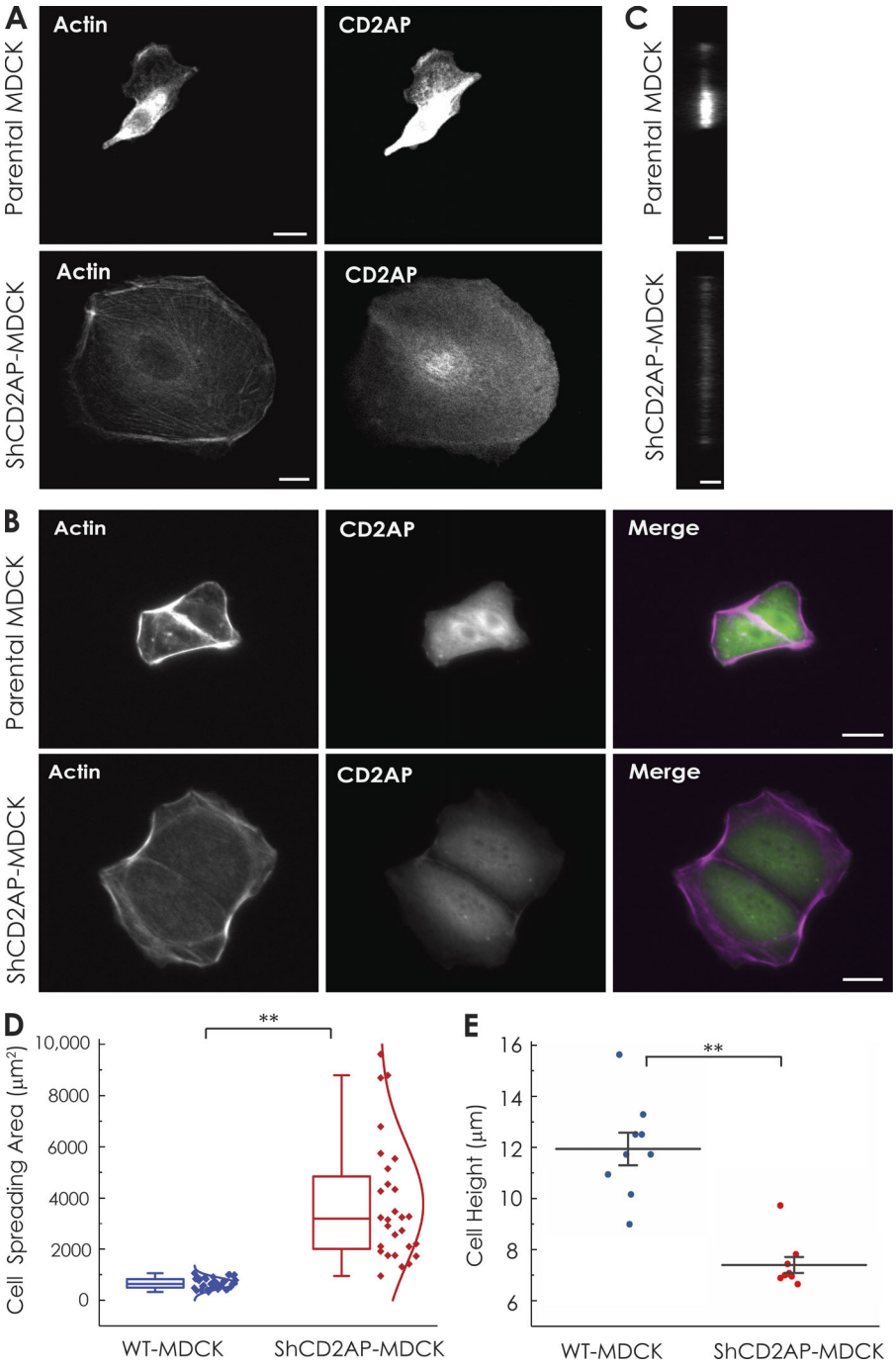

Figure 2. **CD2AP regulates cell morphology independent of cell density. (A and B)** CD2AP knockdown decreases epithelial cell height and expands cell area at the single-cell level. WT (top) and CD2AP-knockdown (bottom) MDCK cells were plated onto glass coverslips at low seeding density for 24 h (A) or 48 h (B) and then fixed and stained for actin and CD2AP. Scale bars, 16 µm. **(C)** Confocal yz sections of WT (top) and CD2AP knockdown (bottom) MDCK cells in A stained with TRITC phalloidin. Scale bars, 9 µm. **(D and E)** Quantification shows that CD2AP depletion results in (D) increased cell spreading area and (E) decreased cell height at the single-cell level. **, $P < 0.05$ (ANOVA). Error bars represent SD from three independent experiments.

in Fig. 4 A, CD2AP knockdown diminished the PI3K p85α signal both underlying the apical cortex and along cell–cell borders. Quantification confirmed the strong correlation between CD2AP and PI3K p85α (Fig. 4, B and C). Similarly, CD2AP knockdown also decreased PI3K p110γ accumulation at cell borders (Fig. 4, D and E). As shown in Fig. 4 F, the p110γ catalytic subunit of PI3K coimmunoprecipitates with CD2AP. Western blots showed the total levels of p85α and 110γ were unaffected by CD2AP depletion (Fig. S1). The dim PI3K signal in CD2AP-knockdown cells is therefore due to its diffuse distribution over a larger area as opposed to a decrease in expression. Thus, CD2AP is necessary for PI3K p85α and p110γ membrane recruitment in MDCK cells.

Loss of PI3K at membranes was accompanied by a decrease in the amount of $PI(3,4,5)P_3$ at lateral membranes as shown by the loss of PH-GFP fluorescent signal at cell boundaries (Fig. 4 G). Line scans across cell boundaries showed a peak of CD2AP fluorescence in register with the PH-GFP peak in WT cells (Fig. 4 H). In contrast, both CD2AP and PH-GFP signals were diminished in CD2AP-depleted cells, and fluorescence intensity across cell boundaries was flat (Fig. 4 H). Population analysis revealed that PH-GFP signals peak in ∼70% of WT-MDCK cells and only ∼13% of shCD2AP-MDCK cells (Fig. 4 I). Fig. 4 J shows aggregate data from different cells plotting the ratio of the peak PH-GFP intensity at the cell–cell boundary to the average

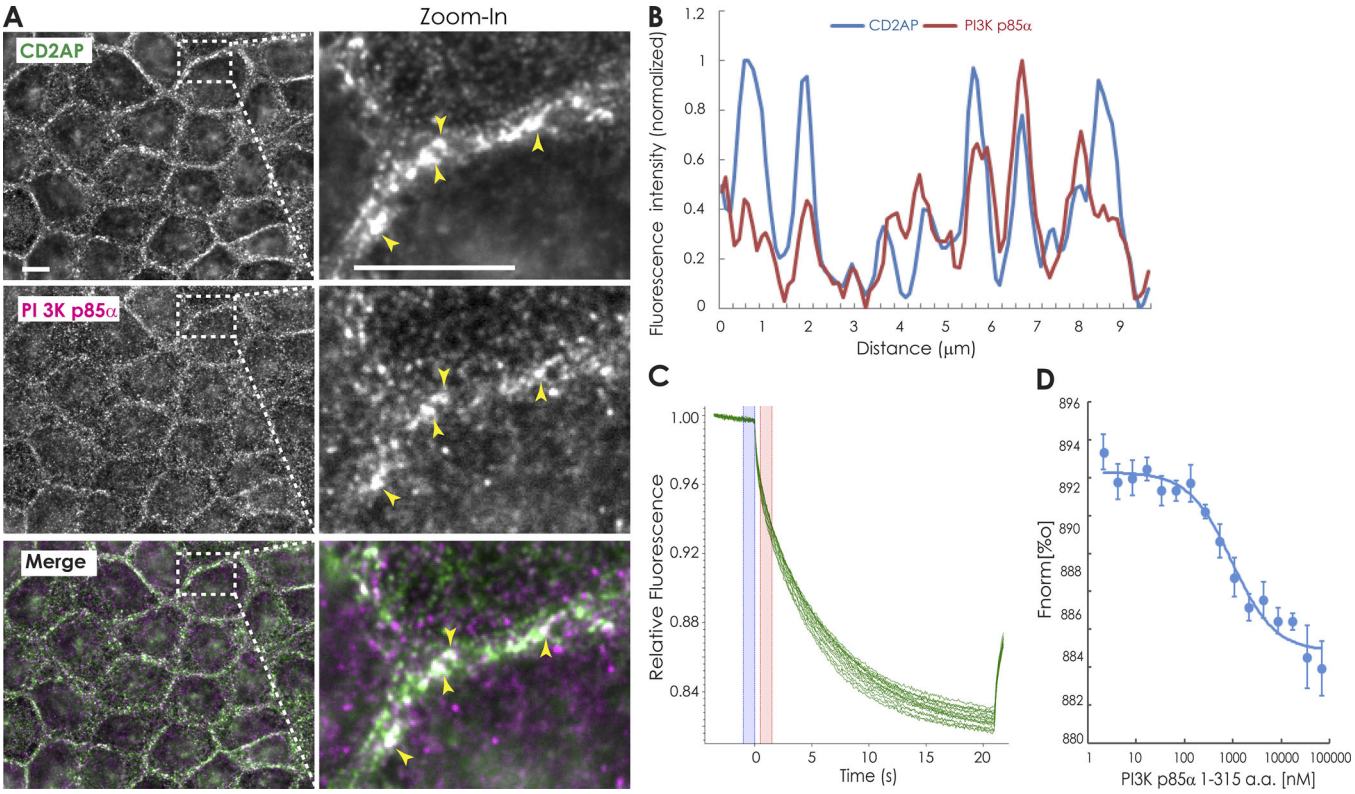

Figure 3. **CD2AP colocalizes with and binds to PI3K p85α at the adherens junction. (A)** Wide-field immunofluorescence images of mature WT-MDCK cells stained for CD2AP (green) and PI3K p85α (magenta). Zoom-in view of dashed white boxes are shown on the right. CD2AP and PI3K p85α partly colocalize at cell–cell borders (arrowheads). Merged images show regions of colocalization (white spots). Scale bar, 10 µm. **(B)** Fluorescence intensity profiles along the indicated lines in A support the partial colocalization of CD2AP and PI3K p85α. **(C)** The association of GFP-CD2AP-1–475 aa with PI3K p85α 1–315 aa was measured by MST. 16 different concentrations (from 2.09 nM to 68.5 µM) of PI3K p85α 1–315 aa were titrated into GFP-CD2AP-1–475 aa (20 nM). Thermophoresis traces shown from one representative experiment are shown. **(D)** Binding isotherm derived from the raw data and fitted to yield a K_d of 0.94 ± 0.41 µM. Error bars represent SD; n = 3.

intensity of PH-GFP in the middle of the cell. Together, the results show that CD2AP is necessary for recruiting PI3K and synthesizing PI(3,4,5)P_3 at cell–cell boundaries.

PI3K is necessary for assembling lateral and apical actin and maintaining cell height

Previous results have shown that the height of the lateral membrane and constraint of the apical and basal surfaces depends on actin nucleation and elongation factors (Yu-Kemp et al., 2017). PI3K is an important activator for actin assembly in many cell types, but its role in maintaining actin assembly in mature epithelial cell sheets is not known. To test this, we treated cells with the PI3K inhibitor LY294002 and used fluorescence microscopy to image actin, CD2AP, and PI3K p85α (Fig. 5 A). Z stacks were collected to measure cell height (Fig. 5 B). The results showed that cell area increased (Fig. 5 C) and cell height decreased (Fig. 5 D) in the presence of the inhibitor, as expected from previous results (Gassama-Diagne et al., 2006; Jeanes et al., 2009). Quantification of fluorescence intensities showed that inhibiting PI3K caused a large drop in both F-actin and PI3K p85α levels at cell boundaries, but the level of CD2AP was unaffected (Fig. 5 E). These results showed that sustained levels of F-actin at cell–cell boundaries in mature epithelial sheets depends on continuous PI3K activity and suggested that PI3K maintains lateral membrane height by activating actin polymerization.

F-actin accumulation reciprocally regulates CD2AP and PI3K levels on lateral membranes

Actin assembly promotes PI3K activity in other systems (Gassama-Diagne et al., 2006; Hawkins et al., 1995; Benard et al., 1999; Weiner et al., 2002; Srinivasan et al., 2003; Welch et al., 2003). We hypothesized that a similar, reciprocal relationship between actin and PI3K activity might exist in epithelial cells. To test this, we treated WT-MDCK cells with latrunculin B (LatB) for 2 h before staining the cells for actin, CD2AP, and the P85α subunit of PI3K (Fig. 6 A). Quantification showed that actin, CD2AP, and PI3K levels significantly dropped upon LatB treatment (Fig. 6, B and C), and this was accompanied by expansion of the cell-spreading area (Fig. 6 D), indicating that actin polymerization can be both upstream and downstream of CD2AP and PI3K (Fig. 6 E).

Effective cell area constriction requires SH3 domains of CD2AP and recruiting PI3K

To better understand the relationships among CD2AP, actin, PI3K, and cell proportions, we performed a structure–function analysis on CD2AP. CD2AP is a modular protein consisting of

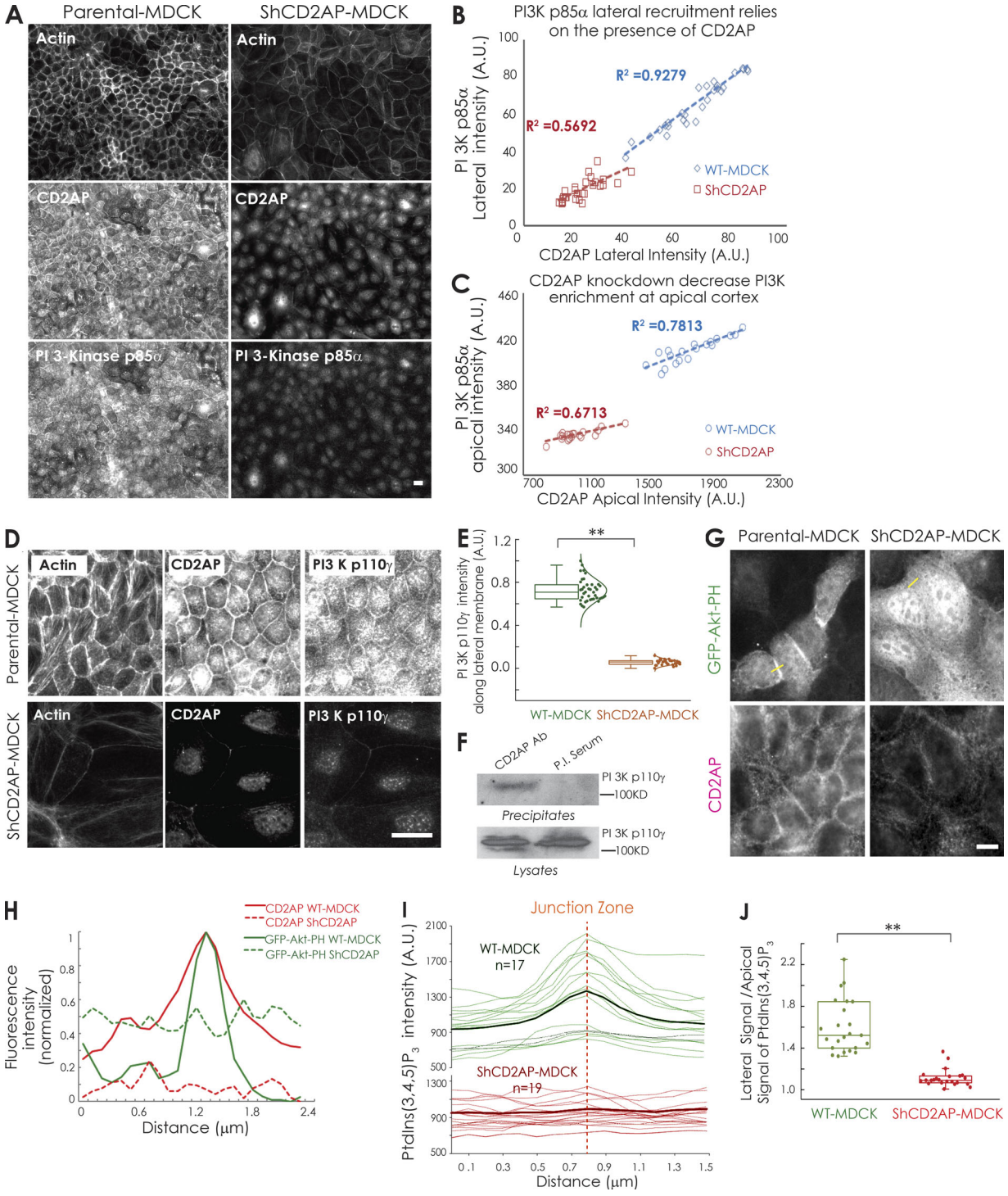

Figure 4. **$PI(3,4,5)P_3$ synthesis and PI3K membrane recruitment is diminished in CD2AP-knockdown MDCK cells. (A)** Wide-field microscopy of WT-MDCK (left panel) and shCD2AP-MDCK cells (right panel) stained for actin, CD2AP, and PI3K p85α showing CD2AP depletion results in compromised membrane recruitment of PI3K p85α. Scale bar, 15 µm. **(B and C)** Quantification of lateral and apical staining of CD2AP and PI3K p85α shows a correlation between CD2AP levels and PI3K p85α levels in both WT and CD2AP-knockdown MDCK cells. R^2 is the coefficient of determination. **(D)** Immunofluorescence of WT-MDCK cells and ShCD2AP-MDCK cells fixed and stained for actin, CD2AP, and PI3K p110γ. Scale bar, 30 µm. **(E)** Quantification of PI3K p110γ at cell borders in D showing CD2AP knockdown decreases PI3K p110γ levels along the lateral membrane. **(F)** WT-MDCK cell lysates were immunoprecipitated with anti-CD2AP antibody (Ab) or preimmune (P.I.) serum, and precipitates (top) or cell lysates (bottom) were stained for PI3K p110γ. **(G)** CD2AP is necessary for $PI(3,4,5)P_3$ accumulation at cell–cell borders. Parental MDCK and shCD2AP-MDCK cells stably transfected with GFP-Akt-PH were fixed and stained for CD2AP. Scale bar, 20 µm. **(H)** GFP-Akt-PH and CD2AP intensity profile across cell borders sampled from the designated line in G showing a peak of $PI(3,4,5)P_3$ coinciding with a peak of CD2AP at cell–cell borders, which is lost in CD2AP-depleted cells. **(I)** Population of line scans of GFP-Akt-PH signal in WT-MDCK and shCD2AP-MDCK cells. Bold lines are the average fluorescence intensities. **(J)** The ratio of lateral/apical GFP-Akt-PH intensity in WT-MDCK and shCD2AP were shown in boxplot. **, $P < 0.001$ by ANOVA. Error bars represent SD from three independent experiments.

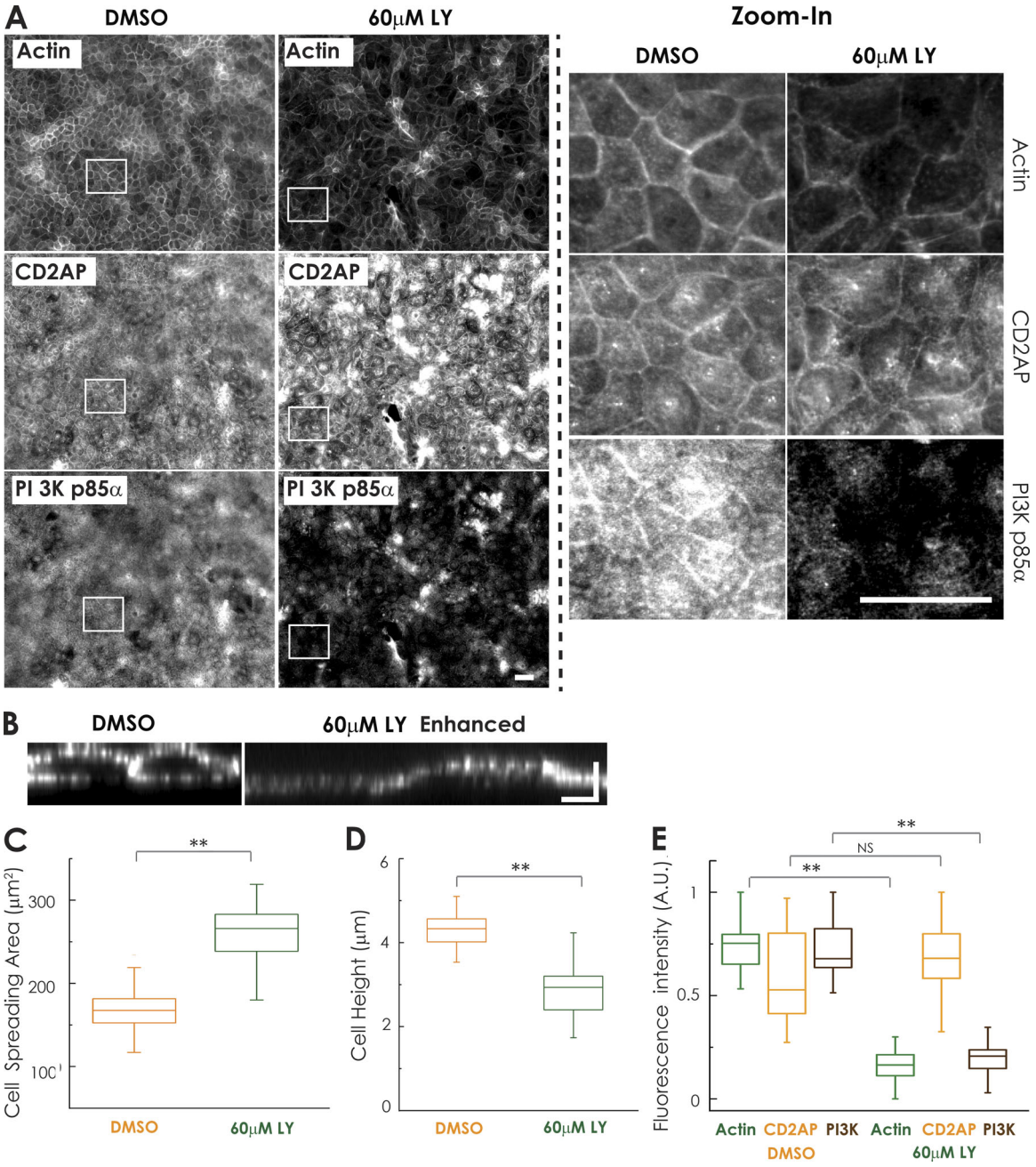

Figure 5. **PI3K inhibition leads to decreased cell height and increased cell-spreading area. (A)** Mature WT-MDCK monolayers were treated for 24 h with 0 and 60 µM LY294002. Cells were then fixed and stained for actin, CD2AP, and PI3K p85α. Zoom-in views of the white boxes are shown on the right. Bar, 30 µm. **(B)** Confocal XZ sections stained with TRITC phalloidin shows LY294002 treatment shortens cell height, the contrast in the right panel has been enhanced. Bar, 4 µm. Quantification of cell XZ and XY dimension shows LY294002 treatment results in (C) increased cell spreading area and, (D) decreased cell height. **, $P < 0.001$ with ANOVA analysis. **(E)** Quantification of actin, CD2AP and PI3K p85α levels shows CD2AP levels are not affected by LY294002 treatment. **, $P < 0.001$ (ANOVA).

three SH3 domains at the N-terminus followed by a proline-rich segment, binding sites for capping protein, and finally a coiled-coil domain near the C-terminus (Fig. 7 A). We made various deletions in CD2AP and then tested the extent to which these deletions could rescue CD2AP-knockdown phenotypes. A schematic of the deletion mutants is shown in Fig. 7 A. Representative images of the actin cytoskeleton in rescued MDCK cells are provided in Fig. 7 B. For quantification, we plotted the actin fluorescence intensity as a function of the fluorescence intensity of the transfected CD2AP construct (Fig. 7, C–H) and also the cell area for each of the deletion constructs (Fig. 7 I). First, we demonstrated that full-length CD2AP rescued both actin assembly and cell area in CD2AP-depleted cells (Fig. 7, B, C, and I). Transfected cells show cytosolic staining of the epitope tag and its accumulation at cell boundaries. Similarly, CD2AP 1–475, which contains only the SH3 domains and the proline-rich

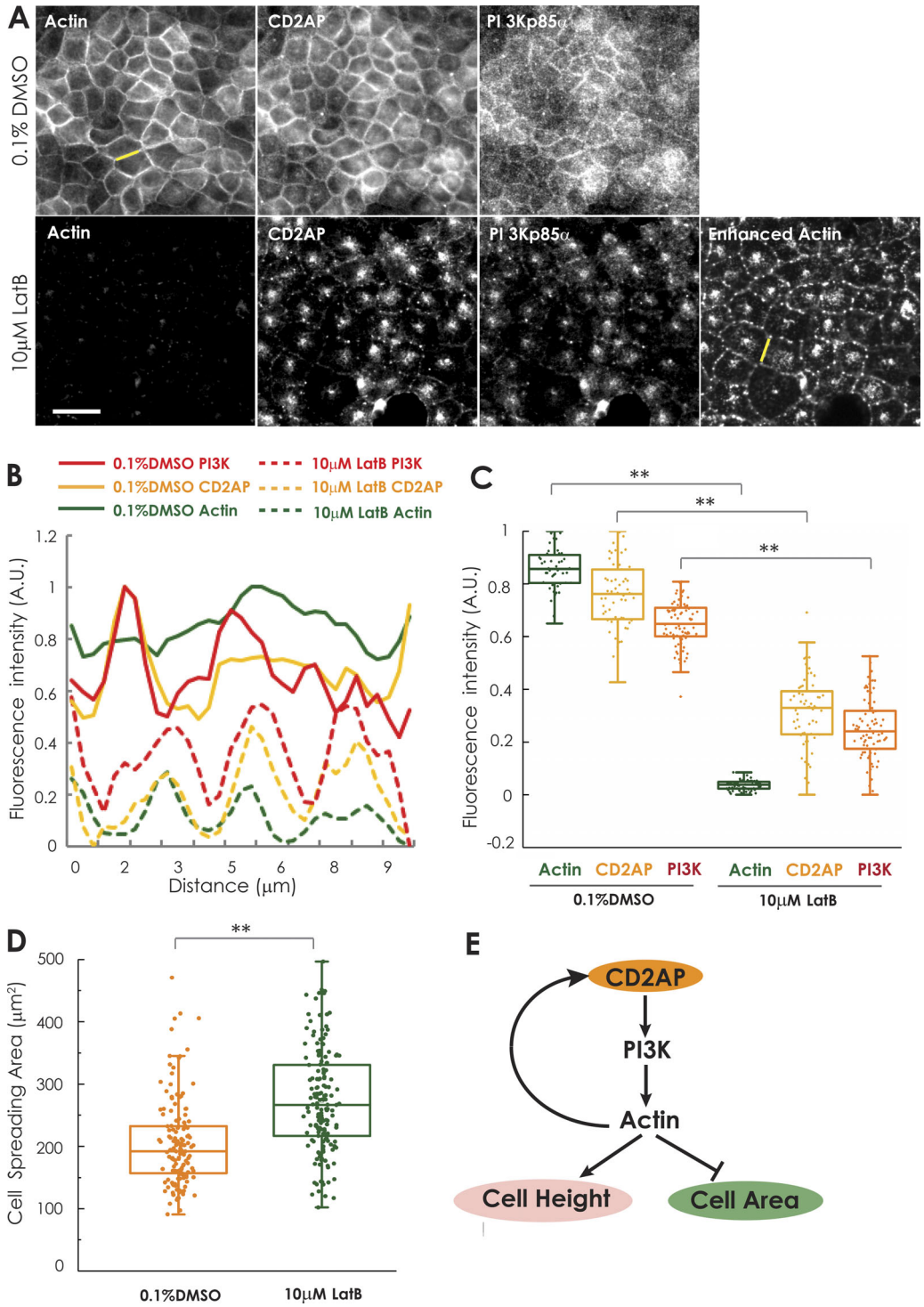

Figure 6. **F-Actin is necessary for recruiting CD2AP and PI3K at cell–cell boundaries. (A)** Loss of CD2AP and PI3K p85 α from cell–cell borders upon exposure to LatB (10 µM) for 2 h. MDCK cells (3 d postconfluent) were treated with 0.1% DMSO or 10 µM LatB in 0.1% DMSO for 2 h and then fixed and triple stained for F-actin, CD2AP, and PI3K p85α. Scale bar, 22 µm. **(B)** Actin, CD2AP, and PI3K p85 α intensity profile along cell borders sampled from the designated yellow lines in A. **(C)** Aggregate data showing loss of actin, CD2AP, and PI3K p85 α in latrunculin-treated cells. **, P < 0.001 (ANOVA). **(D)** Quantification shows that LatB treatment increased cell-spreading area. **, P < 0.001 (ANOVA). **(E)** Schematic model illustrating proposed positive feedback loop involving CD2AP, PI3K, and actin in controlling cell morphology.

domain, rescued actin and appropriate cell area (Fig. 7, B, F, and I). CD2AP constructs lacking either the capping protein or cortactin-binding sites also rescued actin and cell area (Fig. 7, B, D, E, and I). The levels of CD2AP 336–605 were equal to endogenous levels of CD2AP in WT cells. The other constructs we overexpressed ∼24–53% relative to the normal level of

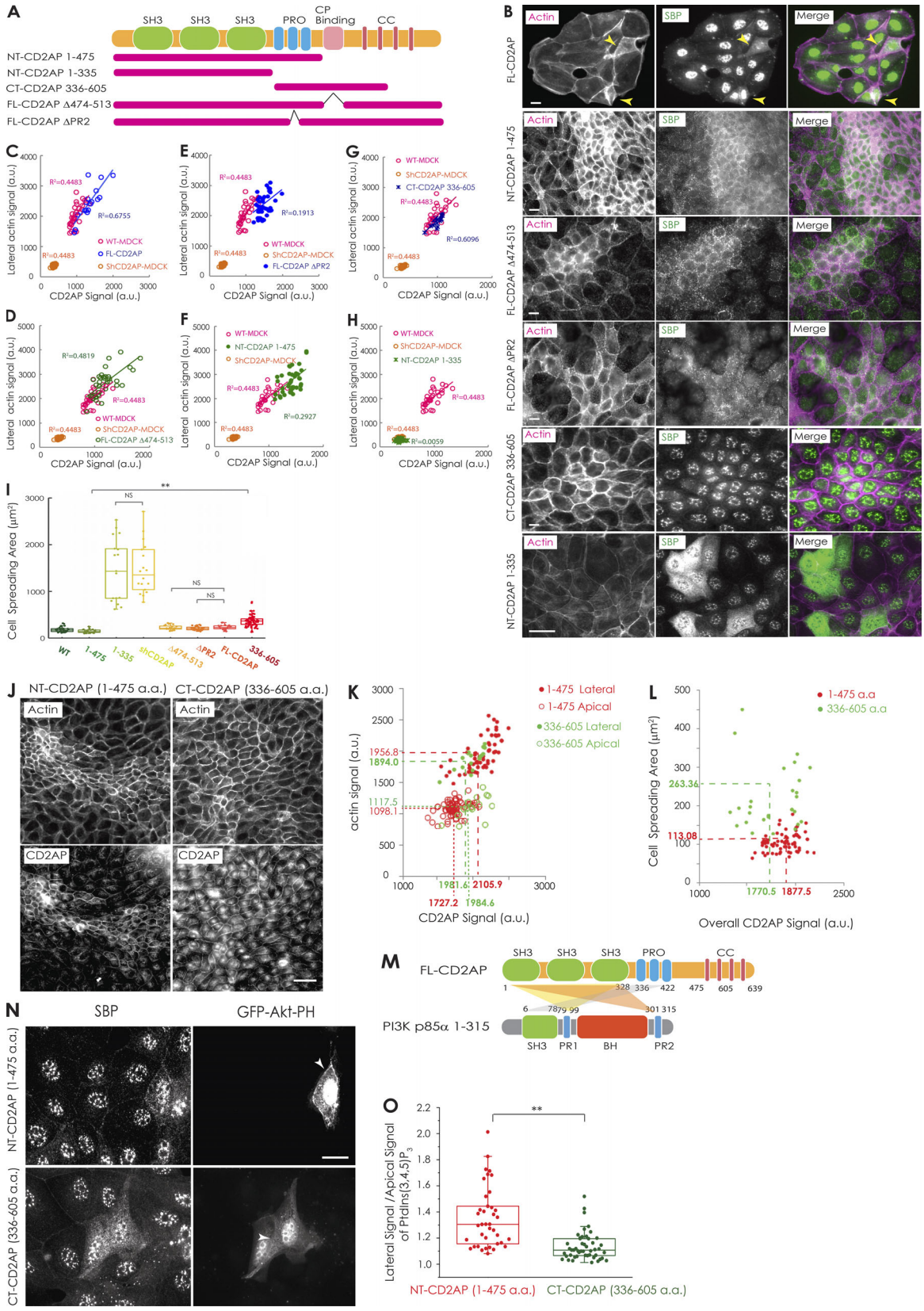

Figure 7. **Effective cell area constriction requires SH3 domains of CD2AP and recruiting PI3K. (A)** Schematic representation of CD2AP constructs. **(B)** shCD2AP-MDCK cells were transfected with FL-CD2AP, CD2AP 1–475 aa, CD2AP CP-binding mutant (Δ474–513 aa), cortactin-binding mutant (Δ377–398 aa), CD2AP 336–605 aa, and CD2AP 1–335 aa and then fixed and stained for actin and SBP-tag to identify the transfected cells. Arrowheads indicate CD2AP-knockdown cells transfected with FL-CD2AP. Bars, 16 µm. **(C–H)** Quantification of lateral staining of actin (phalloidin) and CD2AP levels upon transfection of

various constructs and fitted linear regression showing their different capacities of restoring F-actin in CD2AP-knockdown cells. The expression levels of various CD2AP constructs in shCD2AP cells were similar or higher than that of the endogenous CD2AP in WT cells by immunostaining with CD2AP antibody (except for 1–335 aa, which is not recognized by the CD2AP antibody). **(I)** Quantification of the cell-spreading area upon various constructs transfection in shCD2AP-MDCK cells. Representative data from three separate experiments (n = 3) are shown. **, P ≤ 0.05 (ANOVA). Error bars represent SD from three independent experiments. **(J)** Wide-field immunofluorescence images showing NT-CD2AP restored cell spreading area to a greater extent than CT-CD2AP in shCD2AP-MDCK cells. Scale bar, 33 µm. **(K)** Quantification showing rescue of lateral (solid dots) and apical (open dots) actin levels by NT-CD2AP(red) and CT-CD2AP(green). Dashed lines connect the mean value of the fluorescence intensity of the expressed protein to the mean value of the actin fluorescence intensity. **(L)** Quantification showing rescue of cell-spreading area by NT-CD2AP(red) and CT-CD2AP(green). Dashed lines connect the mean value of the fluorescence intensity of the expressed protein to the mean value of the cell-spreading area. **(M)** Schematic representation of CD2AP and PI3K p85α structures and binding sites. **(N)** shCD2AP-MDCK cells were cotransfected with GFP-Akt-PH and NT-CD2AP (1–475 aa) or CT-CD2AP (336–605 aa), respectively, and then fixed and stained for SBP to mark transfected cells. Arrowheads mark the accumulation of GFP-Akt-PH at cell–cell border in NT-CD2AP transfected cells, but there is no accumulation at cell borders in CT-CD2AP transfected cells. Scale bar, 10 µm. **(O)** The ratio of lateral/apical GFP-Akt-PH intensity in NT-CD2AP and GFP-Akt-PH cotransfected or CT-CD2AP and GFP-Akt-PH cotransfected shCD2AP-MDCK cells is shown in boxplot. **, P ≤ 0.001 (ANOVA).

endogenous CD2AP (Fig. 7, C–F). Linear regression analysis showed that the correlations between the expression levels of these CD2AP constructs with F-actin levels were the same as endogenous CD2AP with F-actin levels in WT-MDCK cells. This suggests that the rescuing constructs restore actin assembly using a mechanism similar to the endogenous CD2AP protein. The strong correlations were seen for every CD2AP construct capable of rescuing actin assembly in CD2AP-knockdown cells with the exception of the CD2AP mutant (Δ378–397/ΔPR2). In this case, the regression relationship suggested that the CD2AP mutant (Δ378–397/ΔPR2), which omitted the cortactin-binding site (Lynch et al., 2003), was less efficient in rescuing F-actin (Fig. 7 E), implying that the CD2AP–cortactin interaction contributes to F-actin accumulation in vivo.

We also identified two informative deletion constructs that failed to rescue cell area. The SH3 domains alone failed to rescue actin assembly or cell area (Fig. 7, B, H, and I). Interestingly, the SH3 domains alone also failed to target to the plasma membrane, whereas all the other constructs that managed to rescue the CD2AP-knockdown phenotype localized to cell–cell boundaries (Fig. S2). In addition, a C-terminal construct lacking the SH3 domains but containing the proline-rich segment and capping protein–binding site rescued actin assembly but was comparatively inefficient in rescuing cell area (Fig. 7, B, G, and I).

We compared the extent of rescue of CD2AP 1–475 to that of CD2AP 336–605, because the N-terminal domain fully rescues the knockdown phenotype while the C-terminal construct exhibits defect in controlling cell dimensions. Fig. 7 J shows fluorescent images of cells from these two rescue experiments side by side. To quantify the relationship between the expression of CD2AP 1–475 or 336–605, we plotted the fluorescent intensity of the deletion constructs versus the actin intensity or cell area. As shown in Fig. 7 K, comparable levels of 1–475 or 336–605 yield comparable levels of F-actin. However, as shown in Fig. 7 L, comparable levels of the two deletion constructs yield different cell areas with 336–605–expressing cells being approximately twofold larger in area than cells expressing the same amount of 1–475. CD2AP 1–475 retains the SH3 domains, which bind to PI3K p85α (Huber et al., 2003), while the 336–605 construct lacks the SH3 domains (Fig. 7 M). As expected, CD2AP 1–475 concentrated PH-GFP fluorescence signals better along cell borders than CD2AP336-605 in shCD2AP-MDCK cells (Figs. 7 N and 5 O). Our data further support the idea that maintaining proper epithelial cell architecture requires CD2AP to bind to and recruit PI3K. Intriguingly, it appears that F-actin assembly per se is not sufficient to support lateral membrane extension, and there might be multiple redundant mechanisms through which CD2AP maintains the actin cytoskeletal network that does or does not involve binding to cortactin.

Targeting the SH3 domains of CD2AP or the catalytic subunit of PI3K to membranes rescues CD2AP knockdown phenotypes

Next, we tested if CD2AP binding to and recruiting PI3K to cell membranes is sufficient to restore normal cell-spreading area in CD2AP-deficient cells. We first confirmed that the three SH3 domains of CD2AP (residues 1–335) interact with PI3K p85α with a K_d = 0.35 ±0.31 µM (n = 3; Fig. S3, A and B). Because the CD2AP 1–335 aa fragment did not localize properly to the membrane (Fig. S3 C), we fused it at the C-terminus to the EGFP-CAAX-box motif and expressed it in shCD2AP-MDCK cells (Fig. S3 D). Our results showed that targeting the SH3 domains of CD2AP to the plasma membrane restored lateral F-actin, PI3K levels, and cell dimensions (Fig. 8, A–C; and Fig. S4). Quantification showed that CD2AP-1-329-EGFP-CAAX expression fully restored F-actin (Fig. 8 D) and PI3K p110γ (Fig. 8 E) intensity along cell borders, and induced 4.9-fold reduction of cell spreading area (from 1,100 ± 447 µm^2 to 226 ± 80 µm^2) in CD2AP-knockdown MDCK cells (Fig. 8 F). To test if recruitment of PI3K to the plasma membrane is sufficient to rescue phenotypes resulting from CD2AP depletion, we targeted the catalytic subunit of PI3K to the plasma membrane using a C-terminal CAAX sequence (p110γ-CAAX; McFall et al., 2001). Cells expressing this construct were difficult to maintain in cell monolayers; therefore, we examined sparsely plated cells. Under such conditions, p110γ-CAAX rescued cell area (Fig. 8, G and H) and F-actin levels (Fig. 8 I) in CD2AP-depleted cells. These results show that a major function of CD2AP in epithelial cell morphology is to recruit PI3K to the membrane, but with the caveat that these membrane-targeting constructs somehow disrupt normal formation of epithelial sheets.

The N-terminal and C-terminal segments of CD2AP bind to F-actin

Previous results showed that CD2AP suppresses the rate of actin assembly in vitro (Tang and Brieher, 2013), but whether this activity is important for CD2AP function in cells is not known. To better understand if there is any relationship between CD2AP-mediated suppression of actin polymerization and

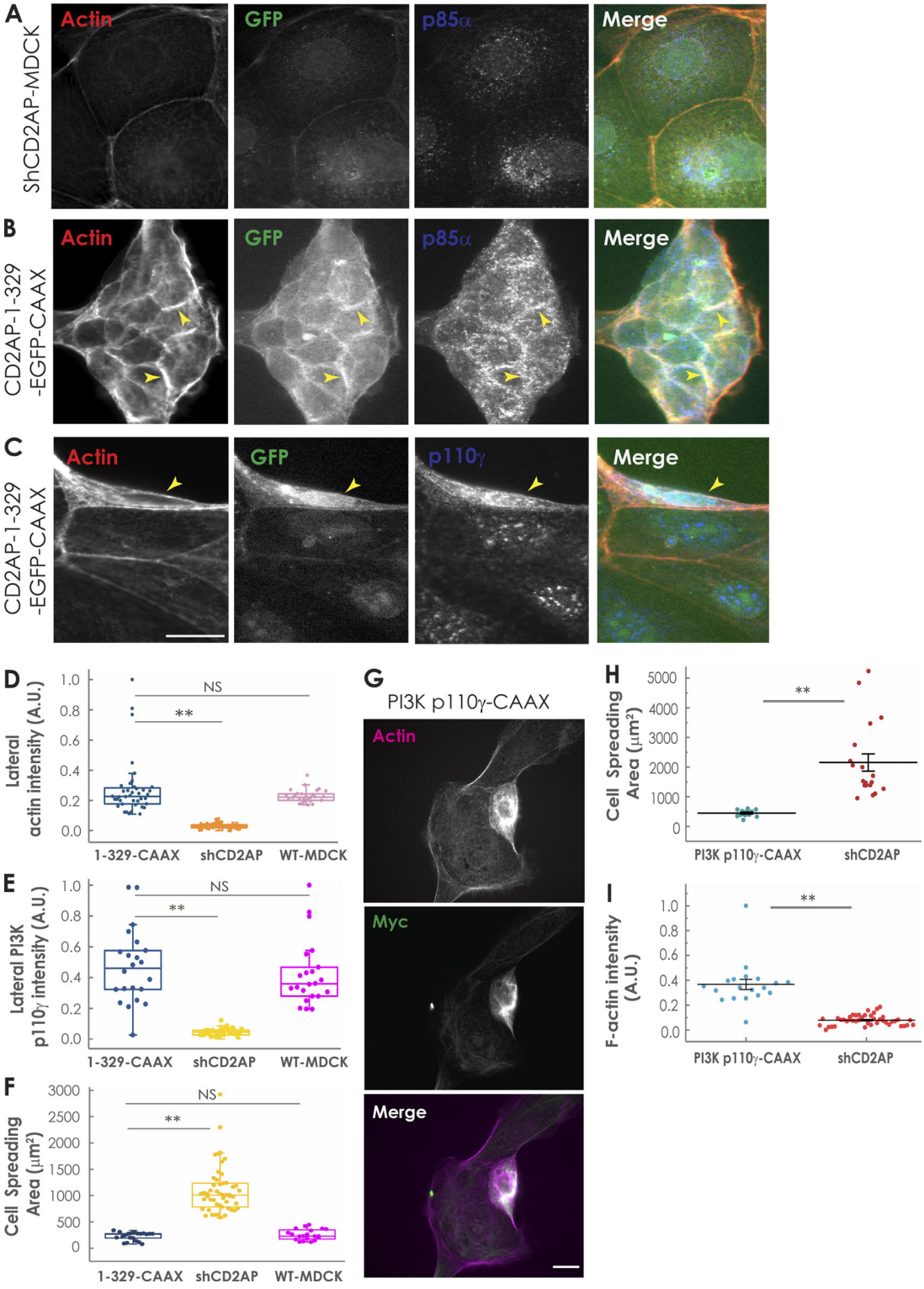

Figure 8. **Targeting the SH3 domains of CD2AP or the catalytic subunit of PI3K to membranes rescues CD2AP knockdown phenotypes. (A)** Immunofluorescence images of shCD2AP-MDCK cells fixed and stained for actin (phalloidin) and PI3K p85α. **(B and C)** shCD2AP-MDCK cells were stably (B) or transiently (C) transfected with CD2AP-1-329-EGFP-CAAX, paraformaldehyde fixed, and stained for actin (phalloidin), PI3K p85α, and p110γ. Scale bar, 16 µm. **(D–F)** Quantification shows CD2AP-1-329-EGFP-CAAX restored lateral actin, lateral p110γ, and cell-spreading area. **, $P < 0.05$ (ANOVA). Representative data from three separate experiments are shown. **(G)** shCD2AP-MDCK cells were transfected with Myc-tagged PI3K p110γ-CAAX 48 h after transfection and then paraformaldehyde fixed and stained for actin (phalloidin) and Myc. Scale bar, 16 µm. **(H and I)** Quantification shows p110γ-CAAX overcame the CD2AP knockdown phenotype. **, $P < 0.05$ (ANOVA).

CD2AP function in cells, we tested the effect of the various CD2AP deletion mutants on actin assembly in vitro. Wide-field fluorescence imaging was used to measure actin polymerization rates in the absence (Fig. 9 A) or presence of CD2AP 1–335 (Fig. 9 B), full-length CD2AP (Fig. 9 C), or CD2AP 1–475 (Fig. 9 E). Rates of actin polymerization were determined from kymographs and plotted (Fig. 9, D and F), which showed that all of these CD2AP constructs inhibited actin assembly. Using MST, we found that CD2AP does not bind to actin monomers at a concentration below 30 µM (Fig. 9, G and H). As a positive control, MST showed that profilin binds to actin monomer with dissociation constant of ∼0.15 µM (Fig. 9, I and J) in agreement with earlier measurements (Vinson et al., 1998). The MST data show that CD2AP is not an actin monomer–sequestering protein, in agreement with previous results (Tang and Brieher, 2013). Pyrene actin assembly was used to confirm that one of the CD2AP constructs, CD2AP 1–475, inhibited actin polymerization in a dose-dependent manner (Fig. 9 K). From the pyrene assays, CD2AP 1–475 was found to inhibit actin assembly with a half maximal inhibitor concentration of ∼5 µM (Fig. 9 L), which is in agreement with results from single-filament imaging (Fig. 9 F). We also confirmed that the C-terminal half of CD2AP (336–605) also inhibits actin assembly (Fig. 9 M). From these results, we can conclude that the ability of CD2AP to suppress actin polymerization is not sufficient to account for the effect of CD2AP on membrane proportions, because 1–335 failed to rescue knockdown phenotypes (Fig. 7, B, H, and I), despite the fact that it inhibited actin filament (+) end assembly. Determining whether CD2AP-mediated suppression of actin filament assembly is necessary for controlling membrane proportions will require more detailed mutagenesis of the three SH3 domains and other sequences within the N-terminal half of the protein.

Discussion

All epithelial cells have to build three different membrane domains, apical, basal, and lateral, each of which performs different functions. While much is known about how each membrane domain is built, little is known about how epithelial cells control the ratios of these three membrane domains. We have identified CD2AP as an important factor in controlling membrane proportions, and Fig. 6 E shows a speculative yet reasonable model for how CD2AP builds up the lateral membrane and restricts the area of the apical membrane. We place CD2AP above PI3K, because targeting the SH3 domains of CD2AP to the membrane rescued $PI(3,4,5)P_3$ accumulation, cell height, and actin assembly in CD2AP-depleted cells (Fig. 8, A–F). We envision the actin cytoskeleton as the downstream effector that converts the PI3K signal into the mechanical work necessary to build up the lateral membrane and constrain cell area. We draw a positive feedback arrow from actin to CD2AP that would yield more PI3K signaling and more actin assembly. Some form of positive feedback from actin to PI3K is justified by our observation that drugging actin assembly blocks PI3K activity at cell–cell boundaries. Actin-dependent activation of PI3K has been seen in several other systems (Gassama-Diagne et al., 2006; Hawkins et al., 1995; Benard et al., 1999; Weiner et al., 2002; Srinivasan et al., 2003; Welch et al., 2003). However, the molecular mechanisms connecting actin to PI3K activation are first being uncovered (Nguyen et al., 2016; Graziano et al., 2017). Drawing the feedback arrow from actin to CD2AP is speculative, but it is supported by the facts that CD2AP binds to both F-actin and PI3K, so more actin polymer mass would create more binding sites for CD2AP and PI3K near the plasma membrane. However, this mechanism is incomplete, because it does not explain why the three SH3 domains of CD2AP alone are not sufficient to rescue all the phenotypes. Rather, the three SH3 domains could rescue actin, PI3K signaling, and cell proportions only when they were experimentally targeted to the membrane. Therefore, additional sequences beyond the SH3 domains are required to properly target CD2AP to lateral membranes. An additional, obvious problem with the model is that it never comes to the steady state. Actin depolymerization, which tends to be proportional to the amount of actin polymer present (Theriot et al., 1992; Kueh et al., 2010), would at least put a brake on runaway lateral membrane production, but ultimately, we expect there to be more layers of signaling loops that control the central machinery shown in Fig. 6 E to establish the appropriate proportions of the three membrane domains. PTEN is a strong candidate for antagonizing the positive feedback loop, because it appears to limit cell height and expand apical area in certain epithelial cells in the prostate (Wang et al., 2006).

The actin cytoskeleton is emerging as a key effector system for building up the lateral membrane and constraining cell area in the plane of the apical and basal membranes. Previous results showed that the actin assembly factors CRMP1, EVL, WAVE2, and Arp2/3 are all necessary for maintaining cell height and constraining cell area (Yu-Kemp et al., 2017), so these proteins are the likely effectors linking CD2AP and PI3K signaling to actin polymerization and cell geometry. All of these actin assembly factors are associated with the formation of branched actin networks that tend to generate protrusive force (Yu-Kemp and Brieher, 2016; Yu-Kemp et al., 2017). Perhaps cells use the energy of actin polymerization to push the lateral membrane up, as hypothesized previously (Tang, 2017), in which case actin along the lateral membrane drives cell height. Alternatively, the actin in the apical membrane, which also depends on CD2AP and the actin assembly factors mentioned above, generates the force to lengthen the lateral membrane. If myosin-dependent contractile forces in the apical actin network were to be exerted on apical cell junctions, those forces could pull the lateral membrane up and pull the apical membrane in to constrain cell area (Tang, 2017). The apical contraction idea is attractive, because it helps explain the role of rho (Yu et al., 2016) and myosin (Kannan and Tang, 2018) in cell height control, and there is strong evidence for tensile forces acting on cell–cell junctions in MDCK cells (Kannan and Tang, 2015; Choi et al., 2016). On the other hand, the basal to apical actin flux seen in certain epithelial cells (Kametani and Takeichi, 2007) is consistent with the pushing idea, and pushing the lateral membrane up might explain why cell-height phenotypes are seen in individual cells and not just confluent sheets. Other mechanisms are possible, including actin-dependent membrane trafficking (Zeng

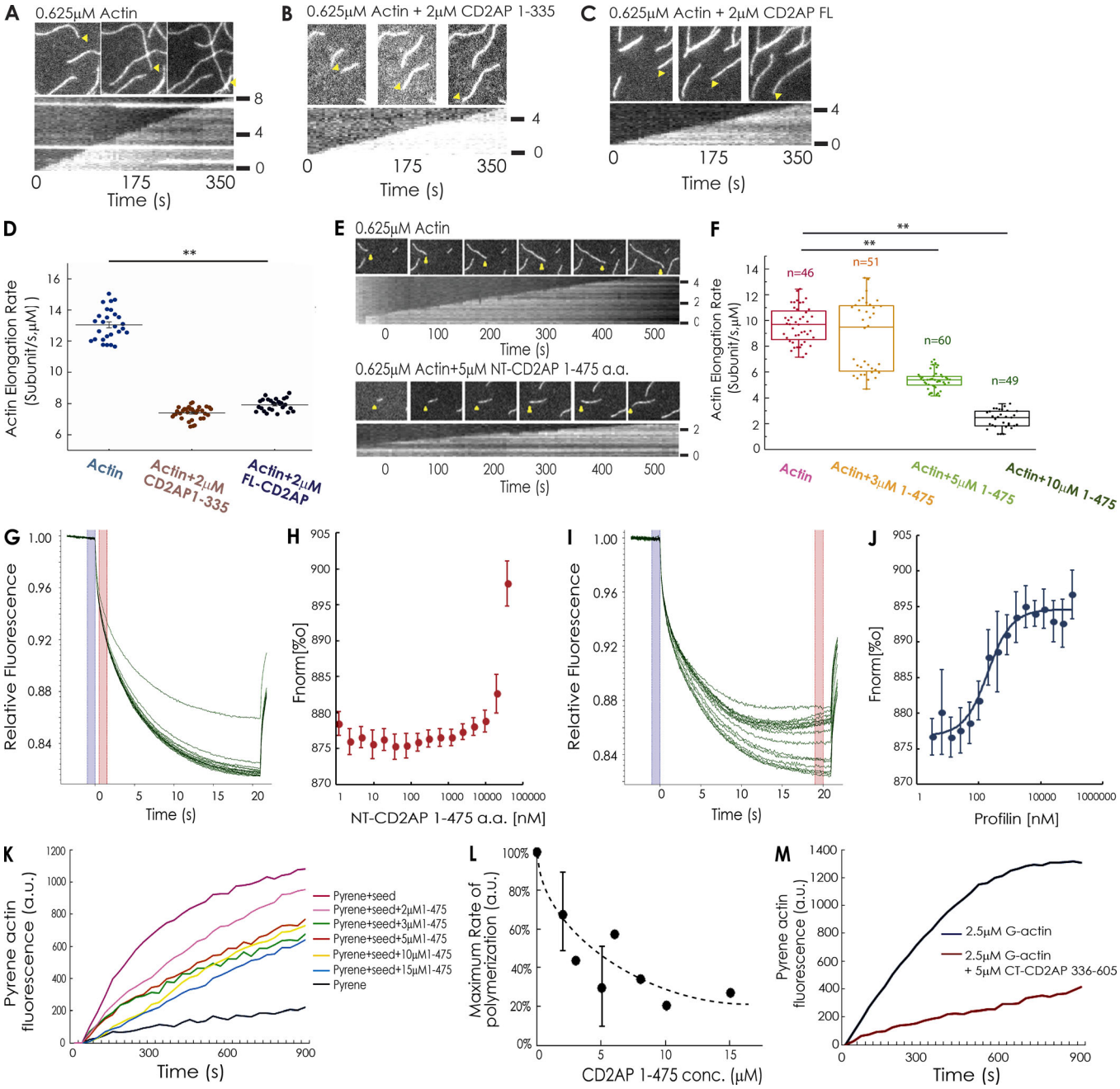

Figure 9. **The N-terminal and C-terminal segments of CD2AP retard actin polymerization in vitro. (A–C)** Frames from wide-field fluorescence time-lapse sequences showing growth of single actin filaments in the absence (A) or presence of 2 µM CD2AP 1–335 (B) or 2 µM FL-CD2AP (C). Arrowheads mark the growing (+) ends of the filament. Representative kymographs of the filaments marked by arrowheads are shown below the frames from the movies. x axis, time (seconds); y axis, length (micrometers). Time beneath the kymographs applies to both the kymographs and the images above them. **(D)** Actin elongation rates were measured by kymograph from single-filament growth time-lapse imaging; boxplot shows that both FL-CD2AP and 1–335 retard actin elongation. **, P ≤ 0.001 (ANOVA). **(E)** Frames from wide-field fluorescence time-lapse sequences showing growth of single actin filaments in the absence (top) or presence (bottom) of 5 µM CD2AP 1–475. Representative kymographs of the filaments marked by arrowheads are shown below the frames from the movies. **(F)** Actin elongation rates were measured by kymograph from single filament growth time-lapse imaging; boxplot shows that increasing concentrations of NT-CD2AP 1–475 aa suppressed actin elongation rates in a dose-dependent manner, **, P ≤ 0.001 (ANOVA). **(G and H)** MST shows no binding of CD2AP to G-actin <30 µM. **(I and J)** Profilin was used as a positive control to show that it binds to G-actin with a K_d of 150.26 ± 62.38 nM. Error bars represent SD; *n* = 3. **(K)** Pyrene-actin spectroscopy assay showing a dose-dependent decrease in spontaneous actin polymerization rate by NT-CD2AP 1–475 aa. Plotted is the fluorescence of pyrene-actin versus time in reactions containing 2.5 µM actin (25% pyrene labeled), 2.5 µM prepolymerized actin seeds. **(L)** The maximum initial polymerization rates were determined from K and plotted against the concentrations of NT-CD2AP 1–475 aa to generate the binding curves. Error bars are the mean values ± SD. **(M)** Pyrene-actin spectroscopy assay shows that CT-CD2AP 336–605 aa decreases spontaneous actin polymerization rate.

et al., 2017). Whatever the precise mechanism, we are at least developing a list of candidate proteins and hypotheses to better explore squamous versus cuboidal versus columnar epithelial morphologies.

Materials and methods

Antibodies and reagents

Antibodies to CD2AP were raised against a synthetic Cys-tagged peptide, EKKYFPIKPEEKDEKSVLEQKPSK, mapping within the C-terminus of canine CD2AP and affinity purified by Pacific Immunology. Antibodies to PI3K p85α (catalog no. 1637, mouse), p110γ (catalog no. 166365, mouse), and SBP (catalog no.101595, mouse) were purchased from Santa Cruz Biotechnology. GAPDH (catalog no. 60004-1-lg, mouse) was purchased from Proteintech. Secondary antibodies were obtained from Bio-Rad Laboratories (HRP anti-rabbit and HRP anti-mouse) and Invitrogen (Alexa Fluor 568 anti-rabbit, Alexa Fluor 647 anti-mouse, and Alexa Fluor 647 phalloidin). FITC-phalloidin, TRITC-phalloidin, and LatB were purchased from Sigma-Aldrich. Protein concentrations were determined by the Bradford or DC Protein Assay (Bio-Rad Laboratories).

DNA constructs

pRS vectors expressing shRNAs targeting N-terminal region of CD2AP were generated as previously described (Tang and Brieher, 2013). pBabe puro pI3K p110 CAAX was obtained from Addgene (catalog no. 13339; McFall et al., 2001). pEGFP-Akt-PH was obtained from Addgene (catalog no. 39533; Watton and Downward, 1999). The coding sequences of human PI3K p85α (catalog no. OHu21143D; GenScript) corresponding to 1–315 aa and various human CD2AP constructs (FL-CD2AP 1–639 aa; CD2AP 1–335 aa, 1–475 aa, 336–605 aa; GFP-1-475 aa; and GFP-1-335 aa) were amplified by PCR (iProof) and cloned in-frame into the bacterial expression vector pET30a+ (EMD) with 6-His tag at the N-terminus for expression in BL21 cells (NEB). CD2AP residues 1–377 and residues 398–639 were fused together to make the FL-CD2AP ΔPR2 cortactin-binding mutant; CD2AP residues 1–474 and 513–639 were fused together to generate the FL-CD2AP Δ474-513 CP-binding mutant. FL-CD2AP (1–639 aa); CD2AP 1–335 aa, 1–329 aa, 1–475 aa, and 336–605 aa; FL-ΔPR2; and FL-Δ474-513 were subcloned into the G418-selectable mammalian expression vector pNTAPB (Agilent Technologies) with a streptavidin-binding peptide tag at the N-terminus for expression in CD2AP-knockdown MDCK cells. EGFP-CaaX was amplified using pEGFP-N1-CIBN-EGFP-Caax (a gift from Chandra Tucker, University of Colorado, Denver, CO) as template and cloned into pNTAPB-CD2AP-1-329 at the C-terminus. CD2AP 336–605 aa, 1–475 aa, and 1–335 aa was subcloned into puromycin-selectable GFP-pLenti-III-HA vector for transient expression in CD2AP-knockdown MDCK cells. All cloning products were verified by ACGT sequencing services.

Cell culture, transfection, and Western blots

MDCK cells (MDCK II) were maintained in MEM (Cell Media Facility, the School of Chemical Sciences, University of Illinois, Urbana-Champaign) supplemented with 5% FBS (Gemini Bio Products). WT and CD2AP-deficient MDCK cells were stably or transiently transfected with plasmids using PolyJet In Vitro DNA Transfection Reagent (SignaGen Laboratories) according to the manufacturer's instructions. Cells were under puromycin (3 μg/ml) or puromycin (3 μg/ml) + G418 (6 μg/ml) selection 24 h after transfection for 14 d. For Western blots, MDCK cells were washed twice and lysed in lysis buffer containing 1% Triton X-100, 1 mM EDTA, 1 mM PMSF, and 1 mM AEBSF. After homogenization, cell lysates were centrifuged at 14,000 ×*g* for 15 min at 4°C, supernatant was collected, protein concentration was determined using the DC Protein Assay, and equal amounts of protein were separated by SDS-10% PAGE. The whole-cell lysates (10–20 μg each) were fractionated in 10% SDS–polyacrylamide gels, transferred to nitrocellulose membranes (GE Healthcare), and blotted with antibodies according to the established procedures. HRP-conjugated IgG antibodies (Bio-Rad) were used as the second antibody. The blots were either exposed to autoradiography film and visualized by chemiluminescence or visualized with iBright Imaging Systems (ThermoFisher Scientific). The amount of α-tubulin or GAPDH detected in the blots was used as an internal control to ensure equal loading of the samples. Three independent Western blots were performed, and representative data are shown.

Protein purification

For expression of recombinant truncation mutants of CD2AP, BL21 cells (NEB) were induced with 500 μM isopropyl β-D-1-thiogalactopyanoside for 7 h at 25°C. Cells were centrifuged at 5,000 rpm for 15 min and resuspended in 20 mM Tris, pH 8.0, 100 mM NaCl, 1 mM EDTA, 40 μM AEBSF, and 10 mg Lysozyme. After a freeze/thaw cycle, lysed cells were centrifuged at 17,000 rpm for 1 h. The supernantant was loaded onto a nickel column (QIAGEN). The column was washed with 10-bed columns of 10 mM Tris, pH 8.0, and 500 mM NaCl; 10-bed columns of 10 mM Tris and 150 mM NaCl; and 20-bed columns of 10 mM Tris, 500 mM NaCl, and 20 mM imidazole, pH 8.0; and eluted with 10-bed volumes of 10 mM Tris, pH 8.0, 150 mM NaCl, and 200 mM imidazole. Protein elutions were concentrated using Centricon (Millipore) and purified by chromatography through a gel filtration column Superdex-200 (GE Healthcare) in 150 mM NaCl, 20 mM Hepes, and 10 mM β-mercaptoethanol. Recombinant actin (Brieher et al., 2004) and filamin (Brieher et al., 2004) were purified as previously described. Actin was labeled with fluorophores as previously described (Brieher et al., 2004).

Immunofluorescence, imaging, and quantitative analyses

MDCK cells grown on coverslips were rinsed twice in PBS and then fixed and permeabilized as previously described (Tang and Brieher, 2013). For Figs. 1 E and 5 B, images were collected with LSM700 confocal microscope (Zeiss) with a NeoFluar 20×/0.5 NA or 63×/1.4 oil differential interference contrast lenses. The Z-section step size was 0.5 μm. Cell height and spreading area were measured randomly throughout the samples while viewing only the channel showing F-actin. Cell height was measured in ImageJ Orthogonal Views xz or yz sections. For other images, fixed cell fluorescence wide-field images were collected with an Axio Imager using AxioVision Release 4.7 with the Colibri

illumination system (Zeiss) using an oil 63× (NA 1.4) or 20× (NA 0.8) objective. Images were acquired using a 1,000 × 1,000 charge-coupled device camera (ORCA-ER; Hamamatsu Photonics). Cell spreading area was measured based on the apical section circumference of individual cells. Composite images were generated using ImageJ software. Images were constructed in Adobe Illustrator. Quantifications and line scans were performed with ImageJ, and OriginLab was used for statistical analyses.

Time-lapse single-filament polymerization assay

0.625 µM Alexa Fluor 647–G-actin (20% labeled) was mixed with FL-CD2AP, CD2AP 1–335, and CD2AP 1–475 at indicated concentrations, and 10 mg/ml bovine casein was allowed to polymerize in photo buffer (Nadkarni and Brieher, 2014; 50 mM KCl, 2 mM $MgCl_2$,1 mM EGTA, 5 mM Hepes, pH 7.2, 2 mM ATP, 0.2 mM 6-hydroxy-2,5,7,8-teramethylchroman-2-carboxylic acid [Trolox], 20 mM imidazole, 4.5 mg/ml glucose, and 0.2 mg/ml glucose oxidase) underneath glasses that were coated with actin-bundling protein α-actinin4. Images were collected every 5 s for 10 min at room temperature with a light microscope (Axio Imager) using the image system described above with the 63× objective lens (NA 1.4). Polymerization rates were determined from kymographs using ImageJ.

Pyrene-actin assays of filament elongation

For Fig. 9 M, pyrene-actin polymerization was monitored in 96-well plates by fluorescence dequenching of pyrene (excitation, 365 nm; emission, 410 nm) upon initiation of actin polymerization in the absence or presence of 5 µM CT-CD2AP 336–605 aa with a SpectraMax M2 plate reader as previously described (Tang and Brieher, 2013).

For Fig. 9 K, the capping rates of the barbed ends of actin seeds were measured as previously described (Huang et al., 2005). Briefly, 2.5 µM unlabeled G-actin was prepolymerized in actin assembly buffer (50 mM KCl, 1 mM EGTA, 2 mM $MgCl_2$, 5 mM Hepes, pH 7.2, 40 mM imidazole, pH 7.0, and 1 mM ATP) to generate actin seeds. Actin seeds (2.5 µM) were mixed with CD2AP 1–475 aa at concentrations indicated in the figure legends before being diluted 10-fold into actin assembly buffer along with 2.5 µM 25% pyrene-labeled G-actin (total volume, 200 µl). The initial rates of polymerization were determined from the increase in pyrene fluorescence E_{x365}/E_{m410} using ImageJ. Readings were normalized using OriginLab software.

Quantification of protein-binding interactions

MST was performed using a Monolith NT.115 instrument (Nanotemper Technologies). MST power was 40%, and excitation power was set to either 20% or 60%. For Fig. 3, C and D, a solution of PI3K p85α 1–335 aa was serially diluted from 68.5 µM to 2 nM in the presence of 20 nM GFP-CD2AP 1–475 aa. For Fig. S3, A and B, PI3K p85α 1–315 aa (from 3.05 nM to 200 µM) was titrated into GFP-CD2AP-1-335 aa (40 nM). For Fig. 9, G and H, CD2AP 1–475 was serially diluted from 38 µM to 1.16 nM in the presence of 100 nM Cy5-G-actin. For Fig. 9, I and J, profilin was serially diluted from 103 µM to 3.13 nM in the presence of 100 nM Cy5-G-actin. The samples were loaded into Monolith NT.115 Standard Treat Capillaries (catalog no. K002; Nanotemper Technologies) and measured in 20 mM Hepes, pH 7.5, with 50 mM NaCl and 0.05% Tween 20. Data were analyzed using Nanotemper Analysis software, v.1.2.101. Error bars represent SD from three independent experiments.

Coimmunoprecipitation

WT-MDCK cells were washed with ice-cold PBS twice, harvested, and hypo-osmotically shocked with 2 mM imidazole, pH 7.4; cells were then lysed in 1% Triton X-100 lysis buffer for 10 min and homogenized through a 25-guage needle on ice. After centrifugation at 14,000 ×*g* (15 min; 4°C), equal amounts of cell lysates were incubated for 1 h at 4°C with CD2AP antibody or preimmune serum (under rotary agitation), followed by incubation with 100 µl protein G-Sepharose beads for 2 h (under rotary agitation). The beads were washed three times with lysis buffer to remove nonspecific binding, and protein complexes were then eluted from the beads by boiling samples in loading buffer with denaturant SDS. Equal amounts of samples were then analyzed by Western blot.

Statistical analysis

All experiments were repeated at least three times. Data distribution was assumed to be normal, but this was not formally tested. One-way ANOVA was performed in OriginLab, P values are indicated in the figure legends, and differences were considered significant at $P \le 0.001$ (**) or $P \le 0.05$ (**). Coefficient of determination R^2 and fitted curves were calculated and generated by Excel and provided in the graphs.

Online supplemental material

Fig. S1 shows that CD2AP knockdown does not affect the total amount of PI3K p85α and PI3K p110γ in shCD2AP-MDCK cells. Fig. S2 shows that GFP-CD2AP-336–605 and GFP-CD2AP-1–475 localize at the cell boundaries. Fig. S3 shows GFP-CD2AP-1–335 binds to PI3K p85α 1–315. CD2AP-1–335 does not localize at cell borders, but CD2AP-1–329-EGFP-CAAX does. Fig. S4 shows that targeting the SH3 domains of CD2AP to the membrane rescues F-actin and PI3K p110γ intensity at cell borders and restores cell morphology.

Acknowledgments

Research reported in this publication was supported by the National Institute of General Medical Sciences of the National Institutes of Health under award number R01GM106106 to W.M. Brieher.

The authors declare no competing financial interests.

Author contributions Y. Wang contributed to methodology, validation, formal analysis, investigation, writing (original draft), and visualization; and W. Brieher contributed to conceptualization, methodology, investigation, writing (review and editing), supervision, project administration, and funding acquisition.

Submitted: 17 December 2018
Revised: 26 August 2019
Accepted: 21 October 2019

References

Benard, V., B.P. Bohl, and G.M. Bokoch. 1999. Characterization of rac and cdc42 activation in chemoattractant-stimulated human neutrophils using a novel assay for active GTPases. *J. Biol. Chem.* 274:13198–13204. https://doi.org/10.1074/jbc.274.19.13198

Bertalanffy, F.D., and C.P. Leblond. 1955. Structure of respiratory tissue. *Lancet.* 269:1365–1368. https://doi.org/10.1016/S0140-6736(55)93164-0

Brieher, W.M., M. Coughlin, and T.J. Mitchison. 2004. Fascin-mediated propulsion of Listeria monocytogenes independent of frequent nucleation by the Arp2/3 complex. *J. Cell Biol.* 165:233–242. https://doi.org/10.1083/jcb.200311040

Bruck, S., T.B. Huber, R.J. Ingham, K. Kim, H. Niederstrasser, P.M. Allen, T. Pawson, J.A. Cooper, and A.S. Shaw. 2006. Identification of a novel inhibitory actin-capping protein binding motif in CD2-associated protein. *J. Biol. Chem.* 281:19196–19203. https://doi.org/10.1074/jbc.M600166200

Caceres, P.S., I. Benedicto, G.L. Lehmann, and E.J. Rodriguez-Boulan. 2017. Directional Fluid Transport across Organ-Blood Barriers: Physiology and Cell Biology. *Cold Spring Harb. Perspect. Biol.* 9:a027847. https://doi.org/10.1101/cshperspect.a027847

Cain, R.J., and A.J. Ridley. 2009. Phosphoinositide 3-kinases in cell migration. *Biol. Cell.* 101:13–29. https://doi.org/10.1042/BC20080079

Choi, W., B.R. Acharya, G. Peyret, M.A. Fardin, R.M. Mège, B. Ladoux, A.S. Yap, A.S. Fanning, and M. Peifer. 2016. Remodeling the zonula adherens in response to tension and the role of afadin in this response. *J. Cell Biol.* 213:243–260. https://doi.org/10.1083/jcb.201506115

Cochran, J.N., T. Rush, S.C. Buckingham, and E.D. Roberson. 2015. The Alzheimer's disease risk factor CD2AP maintains blood-brain barrier integrity. *Hum. Mol. Genet.* 24:6667–6674. https://doi.org/10.1093/hmg/ddv371

Dustin, M.L., M.W. Olszowy, A.D. Holdorf, J. Li, S. Bromley, N. Desai, P. Widder, F. Rosenberger, P.A. van der Merwe, P.M. Allen, and A.S. Shaw. 1998. A novel adaptor protein orchestrates receptor patterning and cytoskeletal polarity in T-cell contacts. *Cell.* 94:667–677. https://doi.org/10.1016/S0092-8674(00)81608-6

Funamoto, S., K. Milan, R. Meili, and R.A. Firtel. 2001. Role of phosphatidylinositol 3′ kinase and a downstream pleckstrin homology domain-containing protein in controlling chemotaxis in dictyostelium. *J. Cell Biol.* 153:795–810. https://doi.org/10.1083/jcb.153.4.795

Funamoto, S., R. Meili, S. Lee, L. Parry, and R.A. Firtel. 2002. Spatial and temporal regulation of 3-phosphoinositides by PI 3-kinase and PTEN mediates chemotaxis. *Cell.* 109:611–623. https://doi.org/10.1016/S0092-8674(02)00755-9

Gassama-Diagne, A., W. Yu, M. ter Beest, F. Martin-Belmonte, A. Kierbel, J. Engel, and K. Mostov. 2006. Phosphatidylinositol-3,4,5-trisphosphate regulates the formation of the basolateral plasma membrane in epithelial cells. *Nat. Cell Biol.* 8:963–970. https://doi.org/10.1038/ncb1461

Graziano, B.R., D. Gong, K.E. Anderson, A. Pipathsouk, A.R. Goldberg, and O.D. Weiner. 2017. A module for Rac temporal signal integration revealed with optogenetics. *J. Cell Biol.* 216:2515–2531. https://doi.org/10.1083/jcb.201604113

Guillot, L., N. Nathan, O. Tabary, G. Thouvenin, P. Le Rouzic, H. Corvol, S. Amselem, and A. Clement. 2013. Alveolar epithelial cells: master regulators of lung homeostasis. *Int. J. Biochem. Cell Biol.* 45:2568–2573. https://doi.org/10.1016/j.biocel.2013.08.009

Hannigan, M., L. Zhan, Z. Li, Y. Ai, D. Wu, and C.K. Huang. 2002. Neutrophils lacking phosphoinositide 3-kinase gamma show loss of directionality during N-formyl-Met-Leu-Phe-induced chemotaxis. *Proc. Natl. Acad. Sci. USA.* 99:3603–3608. https://doi.org/10.1073/pnas.052010699

Hawkins, P.T., A. Eguinoa, R.G. Qiu, D. Stokoe, F.T. Cooke, R. Walters, S. Wennström, L. Claesson-Welsh, T. Evans, M. Symons, and L. Stephens. 1995. PDGF stimulates an increase in GTP-Rac via activation of phosphoinositide 3-kinase. *Curr. Biol.* 5:393–403. https://doi.org/10.1016/S0960-9822(95)00080-7

He, M., K.M. Abdi, and V. Bennett. 2014. Ankyrin-G palmitoylation and βII-spectrin binding to phosphoinositide lipids drive lateral membrane assembly. *J. Cell Biol.* 206:273–288. https://doi.org/10.1083/jcb.201401016

Hernandez-Valladares, M., T. Kim, B. Kannan, A. Tung, A.H. Aguda, M. Larsson, J.A. Cooper, and R.C. Robinson. 2010. Structural characterization of a capping protein interaction motif defines a family of actin filament regulators. *Nat. Struct. Mol. Biol.* 17:497–503. https://doi.org/10.1038/nsmb.1792

Hollingworth, P., D. Harold, R. Sims, A. Gerrish, J.C. Lambert, M.M. Carrasquillo, R. Abraham, M.L. Hamshere, J.S. Pahwa, V. Moskvina, et al. EADI1 consortium. 2011. Common variants at ABCA7, MS4A6A/MS4A4E, EPHA1, CD33 and CD2AP are associated with Alzheimer's disease. *Nat. Genet.* 43:429–435. https://doi.org/10.1038/ng.803

Huang, M., M. Pring, C. Yang, M. Taoka, and S.H. Zigmond. 2005. Presence of a novel inhibitor of capping protein in neutrophil extract. *Cell Motil. Cytoskeleton.* 62:232–243. https://doi.org/10.1002/cm.20097

Huber, T.B., B. Hartleben, J. Kim, M. Schmidts, B. Schermer, A. Keil, L. Egger, R.L. Lecha, C. Borner, H. Pavenstädt, et al. 2003. Nephrin and CD2AP associate with phosphoinositide 3-OH kinase and stimulate AKT-dependent signaling. *Mol. Cell. Biol.* 23:4917–4928. https://doi.org/10.1128/MCB.23.14.4917-4928.2003

Huber, T.B., C. Kwoh, H. Wu, K. Asanuma, M. Gödel, B. Hartleben, K.J. Blumer, J.H. Miner, P. Mundel, and A.S. Shaw. 2006. Bigenic mouse models of focal segmental glomerulosclerosis involving pairwise interaction of CD2AP, Fyn, and synaptopodin. *J. Clin. Invest.* 116:1337–1345. https://doi.org/10.1172/JCI27400

Hutchings, N.J., N. Clarkson, R. Chalkley, A.N. Barclay, and M.H. Brown. 2003. Linking the T cell surface protein CD2 to the actin-capping protein CAPZ via CMS and CIN85. *J. Biol. Chem.* 278:22396–22403. https://doi.org/10.1074/jbc.M302540200

Jeanes, A., M. Smutny, J.M. Leerberg, and A.S. Yap. 2009. Phosphatidylinositol 3′-kinase signalling supports cell height in established epithelial monolayers. *J. Mol. Histol.* 40:395–405. https://doi.org/10.1007/s10735-010-9253-y

Jenkins, P.M., M. He, and V. Bennett. 2015. Dynamic spectrin/ankyrin-G microdomains promote lateral membrane assembly by opposing endocytosis. *Sci. Adv.* 1:e1500301. https://doi.org/10.1126/sciadv.1500301

Kametani, Y., and M. Takeichi. 2007. Basal-to-apical cadherin flow at cell junctions. *Nat. Cell Biol.* 9:92–98. https://doi.org/10.1038/ncb1520

Kannan, N., and V.W. Tang. 2015. Synaptopodin couples epithelial contractility to α-actinin-4-dependent junction maturation. *J. Cell Biol.* 211:407–434. https://doi.org/10.1083/jcb.201412003

Kannan, N., and V.W. Tang. 2018. Myosin-1c promotes E-cadherin tension and force-dependent recruitment of α-actinin to the epithelial cell junction. *J. Cell Sci.* 131:jcs211334. https://doi.org/10.1242/jcs.211334

Kim, J.M., H. Wu, G. Green, C.A. Winkler, J.B. Kopp, J.H. Miner, E.R. Unanue, and A.S. Shaw. 2003. CD2-associated protein haploinsufficiency is linked to glomerular disease susceptibility. *Science.* 300:1298–1300. https://doi.org/10.1126/science.1081068

Kizhatil, K., W. Yoon, P.J. Mohler, L.H. Davis, J.A. Hoffman, and V. Bennett. 2007. Ankyrin-G and beta2-spectrin collaborate in biogenesis of lateral membrane of human bronchial epithelial cells. *J. Biol. Chem.* 282:2029–2037. https://doi.org/10.1074/jbc.M608921200

Kueh, H.Y., W.M. Brieher, and T.J. Mitchison. 2010. Quantitative analysis of actin turnover in Listeria comet tails: evidence for catastrophic filament turnover. *Biophys. J.* 99:2153–2162. https://doi.org/10.1016/j.bpj.2010.07.038

Larsson, L., A. Aperia, and G. Elinder. 1983. Structural and functional development of the nephron. *Acta Paediatr. Scand. Suppl.* 305(s305):56–60. https://doi.org/10.1111/j.1651-2227.1983.tb09860.x

Lowe, J.S., and P.G. Anderson. 2015. Epithelial cells. *In* Stevens & Lowe's Human Histology. Mosby, Philadelphia. 37–54. https://doi.org/10.1016/B978-0-7234-3502-0.00003-6

Lynch, D.K., S.C. Winata, R.J. Lyons, W.E. Hughes, G.M. Lehrbach, V. Wasinger, G. Corthals, S. Cordwell, and R.J. Daly. 2003. A Cortactin-CD2-associated protein (CD2AP) complex provides a novel link between epidermal growth factor receptor endocytosis and the actin cytoskeleton. *J. Biol. Chem.* 278:21805–21813. https://doi.org/10.1074/jbc.M211407200

McFall, A., A. Ulkü, Q.T. Lambert, A. Kusa, K. Rogers-Graham, and C.J. Der. 2001. Oncogenic Ras blocks anoikis by activation of a novel effector pathway independent of phosphatidylinositol 3-kinase. *Mol. Cell. Biol.* 21:5488–5499. https://doi.org/10.1128/MCB.21.16.5488-5499.2001

Monzo, P., N.C. Gauthier, F. Keslair, A. Loubat, C.M. Field, Y. Le Marchand-Brustel, and M. Cormont. 2005. Clues to CD2-associated protein involvement in cytokinesis. *Mol. Biol. Cell.* 16:2891–2902. https://doi.org/10.1091/mbc.e04-09-0773

Nadkarni, A.V., and W.M. Brieher. 2014. Aip1 destabilizes cofilin-saturated actin filaments by severing and accelerating monomer dissociation from ends. *Curr. Biol.* 24:2749–2757. https://doi.org/10.1016/j.cub.2014.09.048

Naj, A.C., G. Jun, G.W. Beecham, L.S. Wang, B.N. Vardarajan, J. Buros, P.J. Gallins, J.D. Buxbaum, G.P. Jarvik, P.K. Crane, et al. 2011. Common variants at MS4A4/MS4A6E, CD2AP, CD33 and EPHA1 are associated with late-onset Alzheimer's disease. *Nat. Genet.* 43:436–441. https://doi.org/10.1038/ng.801

Nguyen, T.T., W.S. Park, B.O. Park, C.Y. Kim, Y. Oh, J.M. Kim, H. Choi, T. Kyung, C.H. Kim, G. Lee, et al. 2016. PLEKHG3 enhances polarized cell migration by activating actin filaments at the cell front. *Proc. Natl. Acad. Sci. USA*. 113:10091–10096. https://doi.org/10.1073/pnas.1604720113

Noren, N.K., B.P. Liu, K. Burridge, and B. Kreft. 2000. p120 catenin regulates the actin cytoskeleton via Rho family GTPases. *J. Cell Biol.* 150:567–580. https://doi.org/10.1083/jcb.150.3.567

Ren, Q., and S. You Yu. 2016. CD2-associated protein participates in podocyte apoptosis via PI3K/Akt signaling pathway. *J. Recept. Signal Transduct. Res.* 36:288–291. https://doi.org/10.3109/10799893.2015.1101137

Shih, N.Y., J. Li, V. Karpitskii, A. Nguyen, M.L. Dustin, O. Kanagawa, J.H. Miner, and A.S. Shaw. 1999. Congenital nephrotic syndrome in mice lacking CD2-associated protein. *Science*. 286:312–315. https://doi.org/10.1126/science.286.5438.312

Srinivasan, S., F. Wang, S. Glavas, A. Ott, F. Hofmann, K. Aktories, D. Kalman, and H.R. Bourne. 2003. Rac and Cdc42 play distinct roles in regulating PI(3,4,5)P3 and polarity during neutrophil chemotaxis. *J. Cell Biol.* 160:375–385. https://doi.org/10.1083/jcb.200208179

Tang, V. 2017. Cell-cell adhesion interface: rise of the lateral membrane. *F1000 Res.* 6:276. https://doi.org/10.12688/f1000research.10680.1

Tang, V.W., and W.M. Brieher. 2012. α-Actinin-4/FSGS1 is required for Arp2/3-dependent actin assembly at the adherens junction. *J. Cell Biol.* 196:115–130. https://doi.org/10.1083/jcb.201103116

Tang, V.W., and W.M. Brieher. 2013. FSGS3/CD2AP is a barbed-end capping protein that stabilizes actin and strengthens adherens junctions. *J. Cell Biol.* 203:815–833. https://doi.org/10.1083/jcb.201304143

Theriot, J.A., T.J. Mitchison, L.G. Tilney, and D.A. Portnoy. 1992. The rate of actin-based motility of intracellular Listeria monocytogenes equals the rate of actin polymerization. *Nature*. 357:257–260. https://doi.org/10.1038/357257a0

Van Itallie, C.M., A.J. Tietgens, E. Krystofiak, B. Kachar, and J.M. Anderson. 2015. A complex of ZO-1 and the BAR-domain protein TOCA-1 regulates actin assembly at the tight junction. *Mol. Biol. Cell.* 26:2769–2787. https://doi.org/10.1091/mbc.E15-04-0232

Vinson, V.K., E.M. De La Cruz, H.N. Higgs, and T.D. Pollard. 1998. Interactions of Acanthamoeba profilin with actin and nucleotides bound to actin. *Biochemistry*. 37:10871–10880. https://doi.org/10.1021/bi980093l

Wang, S., A.J. Garcia, M. Wu, D.A. Lawson, O.N. Witte, and H. Wu. 2006. Pten deletion leads to the expansion of a prostatic stem/progenitor cell subpopulation and tumor initiation. *Proc. Natl. Acad. Sci. USA*. 103:1480–1485. https://doi.org/10.1073/pnas.0510652103

Watton, S.J., and J. Downward. 1999. Akt/PKB localisation and 3′ phosphoinositide generation at sites of epithelial cell-matrix and cell-cell interaction. *Curr. Biol.* 9:433–436. https://doi.org/10.1016/S0960-9822(99)80192-4

Weber, K.L., R.S. Fischer, and V.M. Fowler. 2007. Tmod3 regulates polarized epithelial cell morphology. *J. Cell Sci.* 120:3625–3632. https://doi.org/10.1242/jcs.011445

Weiger, M.C., and C.A. Parent. 2012. Phosphoinositides in chemotaxis. *Subcell. Biochem.* 59:217–254. https://doi.org/10.1007/978-94-007-3015-1_7

Weiner, O.D., P.O. Neilsen, G.D. Prestwich, M.W. Kirschner, L.C. Cantley, and H.R. Bourne. 2002. A PtdInsP(3)- and Rho GTPase-mediated positive feedback loop regulates neutrophil polarity. *Nat. Cell Biol.* 4:509–513. https://doi.org/10.1038/ncb811

Welch, H.C., W.J. Coadwell, L.R. Stephens, and P.T. Hawkins. 2003. Phosphoinositide 3-kinase-dependent activation of Rac. *FEBS Lett.* 546:93–97. https://doi.org/10.1016/S0014-5793(03)00454-X

Yu, H.H., M.R. Dohn, N.O. Markham, R.J. Coffey, and A.B. Reynolds. 2016. p120-catenin controls contractility along the vertical axis of epithelial lateral membranes. *J. Cell Sci.* 129:80–94. https://doi.org/10.1242/jcs.177550

Yu-Kemp, H.C., and W.M. Brieher. 2016. Collapsin Response Mediator Protein-1 Regulates Arp2/3-dependent Actin Assembly. *J. Biol. Chem.* 291:658–664. https://doi.org/10.1074/jbc.C115.689265

Yu-Kemp, H.C., J.P. Kemp Jr., and W.M. Brieher. 2017. CRMP-1 enhances EVL-mediated actin elongation to build lamellipodia and the actin cortex. *J. Cell Biol.* 216:2463–2479. https://doi.org/10.1083/jcb.201606084

Zeng, J., S. Feng, B. Wu, and W. Guo. 2017. Polarized Exocytosis. *Cold Spring Harb. Perspect. Biol.* 9. a027870. https://doi.org/10.1101/cshperspect.a027870

Zhai, X.Y., H. Birn, K.B. Jensen, J.S. Thomsen, A. Andreasen, and E.I. Christensen. 2003. Digital three-dimensional reconstruction and ultrastructure of the mouse proximal tubule. *J. Am. Soc. Nephrol.* 14:611–619. https://doi.org/10.1097/01.ASN.0000051725.00406.0C

Zhai, X.Y., J.S. Thomsen, H. Birn, I.B. Kristoffersen, A. Andreasen, and E.I. Christensen. 2006. Three-dimensional reconstruction of the mouse nephron. *J. Am. Soc. Nephrol.* 17:77–88. https://doi.org/10.1681/ASN.2005080796

Zhao, J., S. Bruck, S. Cemerski, L. Zhang, B. Butler, A. Dani, J.A. Cooper, and A.S. Shaw. 2013. CD2AP links cortactin and capping protein at the cell periphery to facilitate formation of lamellipodia. *Mol. Cell. Biol.* 33:38–47. https://doi.org/10.1128/MCB.00734-12

Supplemental material

Wang and Brieher, https://doi.org/10.1083/jcb.201812087

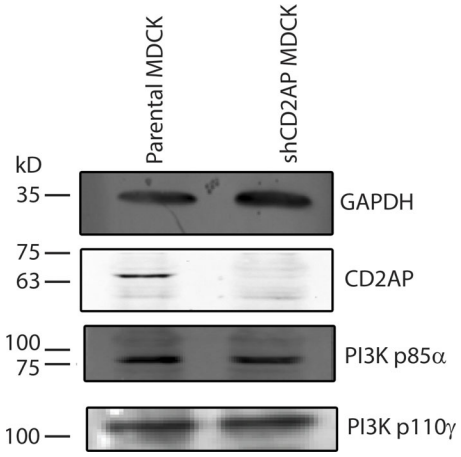

Figure S1. **Western blots of total cell extracts showing that CD2AP knockdown does not affect total amounts of PI3K p85α and p110γ in shCD2AP-MDCK cells.**

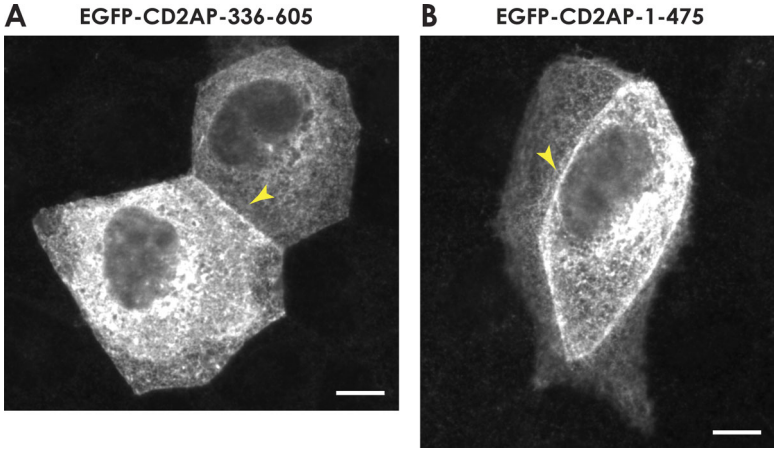

Figure S2. **C-terminal and N-terminal fragments of CD2AP target to the cell membrane.** shCD2AP-MDCK cells were transfected with GFP-CD2AP-336–605 (A) or GFP-CD2AP-1–475 (B) and plated onto glass coverslips. Arrowheads indicate cell–cell boundaries. Wide-field fluorescence images were taken 4 d after transfection. Scale bars, 8 µm.

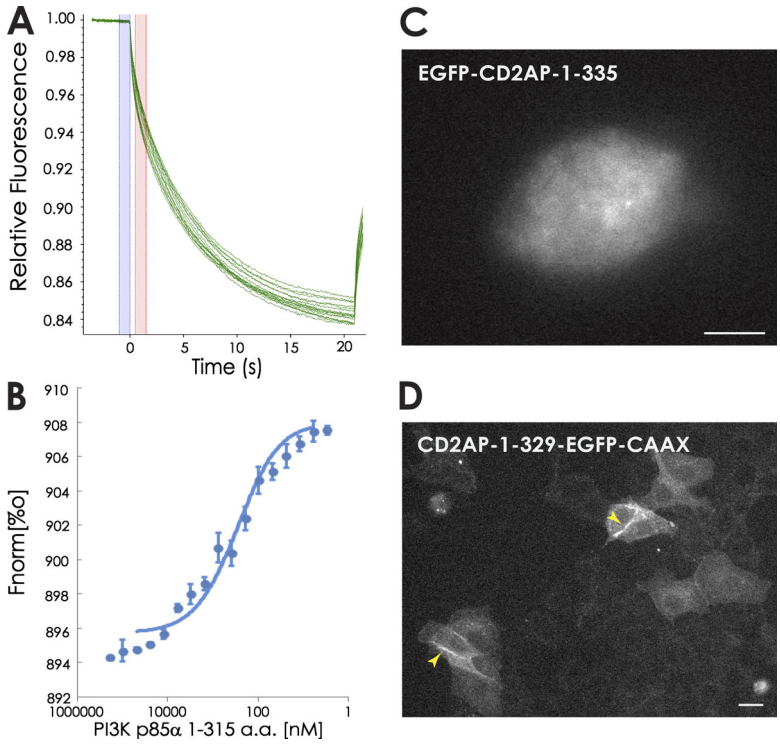

Figure S3. **CD2AP SH3 domains do not localize at the cell membrane, but associate with PI3K p85α. (A)** The association of GFP-CD2AP-1-335 aa with PI3K p85α 1–315 aa was measured by MST. PI3K p85α 1–315 aa (from 3.05 nM to 200 µM) was titrated into GFP-CD2AP-1–335 aa (40 nM). Thermophoresis trace shown from one representative experiment is shown. **(B)** Binding isotherm derived from the raw data and fitted to yield a K_d of 0.35 ± 0.31 µM (n = 3). Error bars represent SD; n = 3. **(C)** shCD2AP-MDCK cells transiently transfected with EGFP-CD2AP-1–335 aa Wide-field microscopy image showing defective CD2AP 1–335 aa recruitment to cell borders. Scale bar, 16 µm. **(D)** shCD2AP-MDCK cells stably transfected with CD2AP-1–329-EGFP-CAAX constructs, which were clearly located at cell borders as indicated by the fluorescence microscopy imaging (arrowheads). Scale bar, 16 µm.

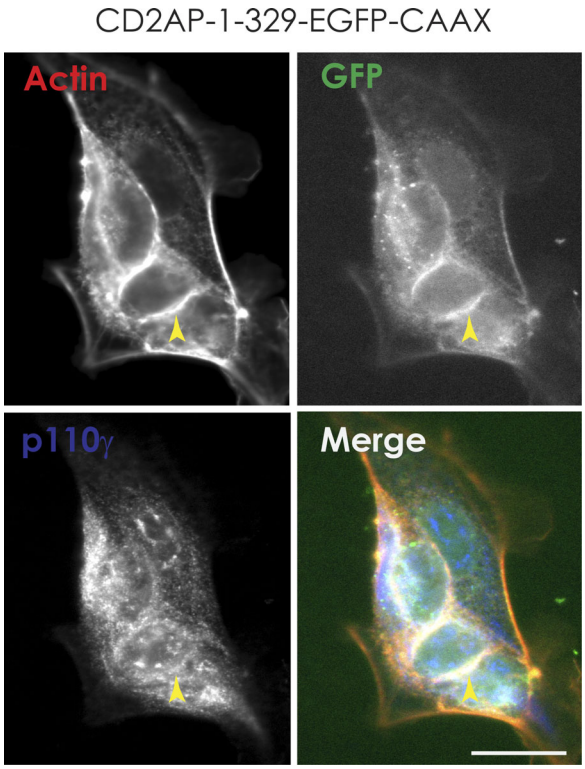

Figure S4. **shCD2AP-MDCK cells were stably transfected with EGFP-CD2AP-1–329-EGFP-CAAX, paraformaldehyde fixed, and stained for actin (phalloidin) and p110γ.** Arrowheads indicate cell–cell boundaries. Scale bar, 16 µm.